Theoretical Seismology

Astrophysics and Cosmology and Earth and Environmental Physics

Seismic sources 3: focal mechanisms

Fabio ROMANELLI

Department of Mathematics & Geosciences

University of Trieste

romanel@units.it

Seismic sources - 3

Focal mechanisms

- faulting and radiation pattern
- fault mechanism
- decomposition of moment tensor
- basic fault plane solutions
- faults and plates

Haskell model

- far field for an extended source
- directivity
- source spectra

Final source representation

$$u_n(x,t) = \iint_\Sigma [u_i] c_{ijpq} \nu_j * \frac{\partial G_{np}}{\partial \xi_q} d\Sigma$$

$$m_{pq} = [u_i] c_{ijpq} \nu_j \qquad u_n(x,t) = \iint_\Sigma m_{pq} * \frac{\partial G_{np}}{\partial \xi_q} d\Sigma$$

And if the source can be considered a point-source (for distances greater than fault dimensions), the contributions from different surface elements can be considered in phase. Thus for an effective **point source**, one can define the **moment tensor**:

$$\boxed{\begin{gathered} M_{pq} = \iint_\Sigma m_{pq} \, d\Sigma \\ u_n(x,t) = M_{pq} * G_{np,q} \end{gathered}}$$

A particular case - moment tensor

$$\mathbf{m}=\begin{pmatrix} 0 & 0 & \mu[u_1(\xi,\tau)] \\ 0 & 0 & 0 \\ \mu[u_1(\xi,\tau)] & 0 & 0 \end{pmatrix} \qquad \mathbf{M}=\begin{pmatrix} 0 & 0 & M_0 \\ 0 & 0 & 0 \\ M_0 & 0 & 0 \end{pmatrix}$$

ϕ=0°, δ=0°, λ°=0°

$$\mathbf{u}=\begin{cases}[\bar{u}]\hat{\mathbf{e}}_x \\ 0 \\ 0\end{cases} \qquad \boldsymbol{\nu}=\begin{cases}0 \\ 0 \\ \hat{\mathbf{e}}_z\end{cases} \qquad \begin{cases}\mathbf{t}=\dfrac{1}{\sqrt{2}}\left(\hat{\mathbf{e}}_z+[\bar{u}]\hat{\mathbf{e}}_x\right) \\ \mathbf{b}=\left(\hat{\mathbf{e}}_z\times[\bar{u}]\hat{\mathbf{e}}_x\right)=[\bar{u}]\hat{\mathbf{e}}_y \\ \mathbf{p}=\dfrac{1}{\sqrt{2}}\left(\hat{\mathbf{e}}_z-[\bar{u}]\hat{\mathbf{e}}_x\right)\end{cases}$$

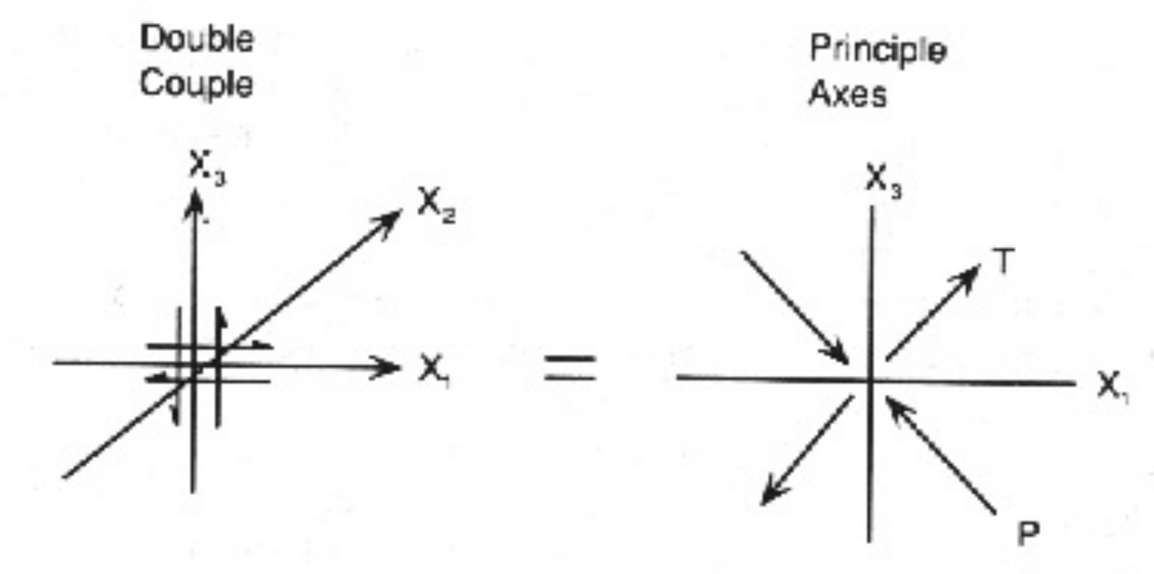

referred to
principal axes

$$\mathbf{M}=\begin{pmatrix} M_0 & 0 & 0 \\ 0 & 0 & 0 \\ 0 & 0 & -M_0 \end{pmatrix}$$

GF for double couple

An important case to consider in detail is the radiation pattern expected when the source is a double-couple. The result for a moment time function $M_0(t)$ is:

$$u = \frac{A^{NF}}{4\pi\rho|\mathbf{x}|^4}\int_{|\mathbf{x}|/\alpha}^{|\mathbf{x}|/\beta}\tau M_0(t-\tau)d\tau + \frac{A_P^{IF}}{4\pi\rho\alpha^2|\mathbf{x}|^2}M_0\left(t-\frac{|\mathbf{x}|}{\alpha}\right) - \frac{A_S^{IF}}{4\pi\rho\beta^2|\mathbf{x}|^2}M_0\left(t-\frac{|\mathbf{x}|}{\beta}\right) + \frac{A_P^{FF}}{4\pi\rho\alpha^3|\mathbf{x}|}\boxed{\dot{M}_0}\left(t-\frac{|\mathbf{x}|}{\alpha}\right) - \frac{A_S^{FF}}{4\pi\rho\beta^3|\mathbf{x}|}\boxed{\dot{M}_0}\left(t-\frac{|\mathbf{x}|}{\beta}\right)$$

$$A^{NF} = 9\sin 2\theta\cos\phi\,\hat{\mathbf{r}} - 6\left(\cos 2\theta\cos\phi\,\hat{\boldsymbol{\theta}} - \cos\theta\sin\phi\,\hat{\boldsymbol{\phi}}\right)$$

Near field term

$$A_P^{IF} = 4\sin 2\theta\cos\phi\,\hat{\mathbf{r}} - 2\left(\cos 2\theta\cos\phi\,\hat{\boldsymbol{\theta}} - \cos\theta\sin\phi\,\hat{\boldsymbol{\phi}}\right)$$

$$A_S^{IF} = -3\sin 2\theta\cos\phi\,\hat{\mathbf{r}} + 3\left(\cos 2\theta\cos\phi\,\hat{\boldsymbol{\theta}} - \cos\theta\sin\phi\,\hat{\boldsymbol{\phi}}\right)$$

Intermediate field term

$$A_P^{FF} = \sin 2\theta\cos\phi\,\hat{\mathbf{r}}$$

$$A_S^{FF} = \cos 2\theta\cos\phi\,\hat{\boldsymbol{\theta}} - \cos\theta\sin\phi\,\hat{\boldsymbol{\phi}}$$

Far field term

Faulting and Seismograms

- The nature of faulting affects the amplitudes and shapes of seismic waves (this allows us to use seismograms to study the faulting).

- We call the variation in wave amplitude, due to the source, with direction (i.e. angular) the **radiation pattern**.

Far field for a point DC point source

From the representation theorem we have: $u_n(\mathbf{x},t) = M_{pq} * G_{np,q}$

that, in the far field and in a spherical coordinate system becomes:

$$\mathbf{u}(\mathbf{x},t) = \frac{1}{4\pi\rho\alpha^3}\left(\sin 2\theta \cos\phi \hat{\mathbf{r}}\right)\frac{\dot{M}(t - r/\alpha)}{r} +$$

$$\frac{1}{4\pi\rho\beta^3}\left(\cos 2\theta \cos\phi \hat{\boldsymbol{\theta}} - \cos\theta \sin\phi \hat{\boldsymbol{\phi}}\right)\frac{\dot{M}(t - r/\beta)}{r}$$

and both P and S radiation fields are proportional to the time derivative of the moment function (moment rate). If the moment function is a ramp of duration τ (**rise time**), the propagating disturbance in the far-field will be a **boxcar**, with the same duration, and whose amplitude is varying depending on the radiation pattern.

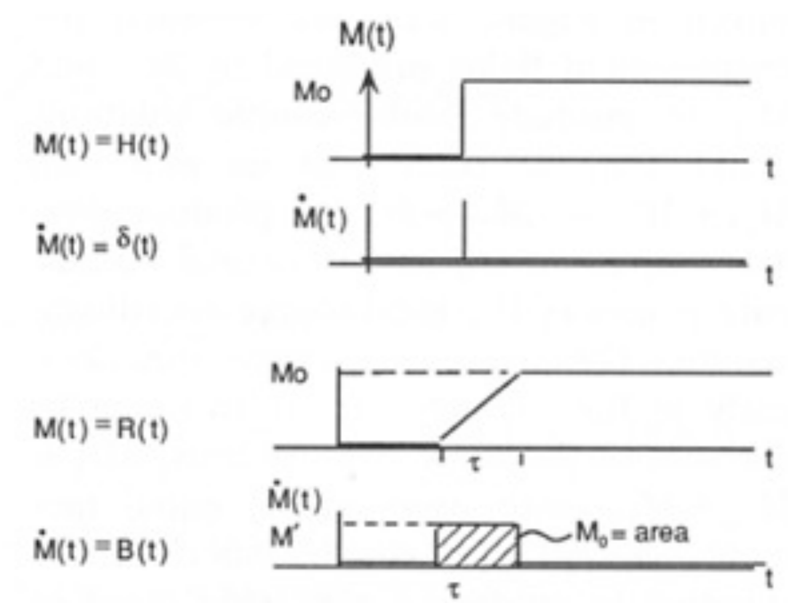

FIGURE 8.21 Far-field *P*- and *S*-wave displacements are proportional to $\dot{M}(t)$, the time derivative of the moment function $M(t) = \mu A(t)D(t)$. Simple step and ramp moment functions generate far-field impulses or boxcar ground motions.

P-wave radiation amplitude patterns:

$$u_r = \frac{1}{4\pi\rho\alpha^3 r}\,\dot{M}(t - r/\alpha)\sin 2\theta\cos\phi.$$

$$\frac{1}{4\pi\rho\alpha^3 r} = \text{ amplitude term, with geometric spreading}$$

$\sin 2\theta \cos\phi =$ P-wave radiation pattern (4-lobed)

$\dot{M}(t - r/\alpha) =$ source time function

$\dot{M}$ is the time derivative of the seismic moment function,

$$M(t) = \mu D(t)S(t)$$

$D(t)$ = slip history
$S(t)$ = fault area history

: Body-wave radiation patterns for a double couple source.

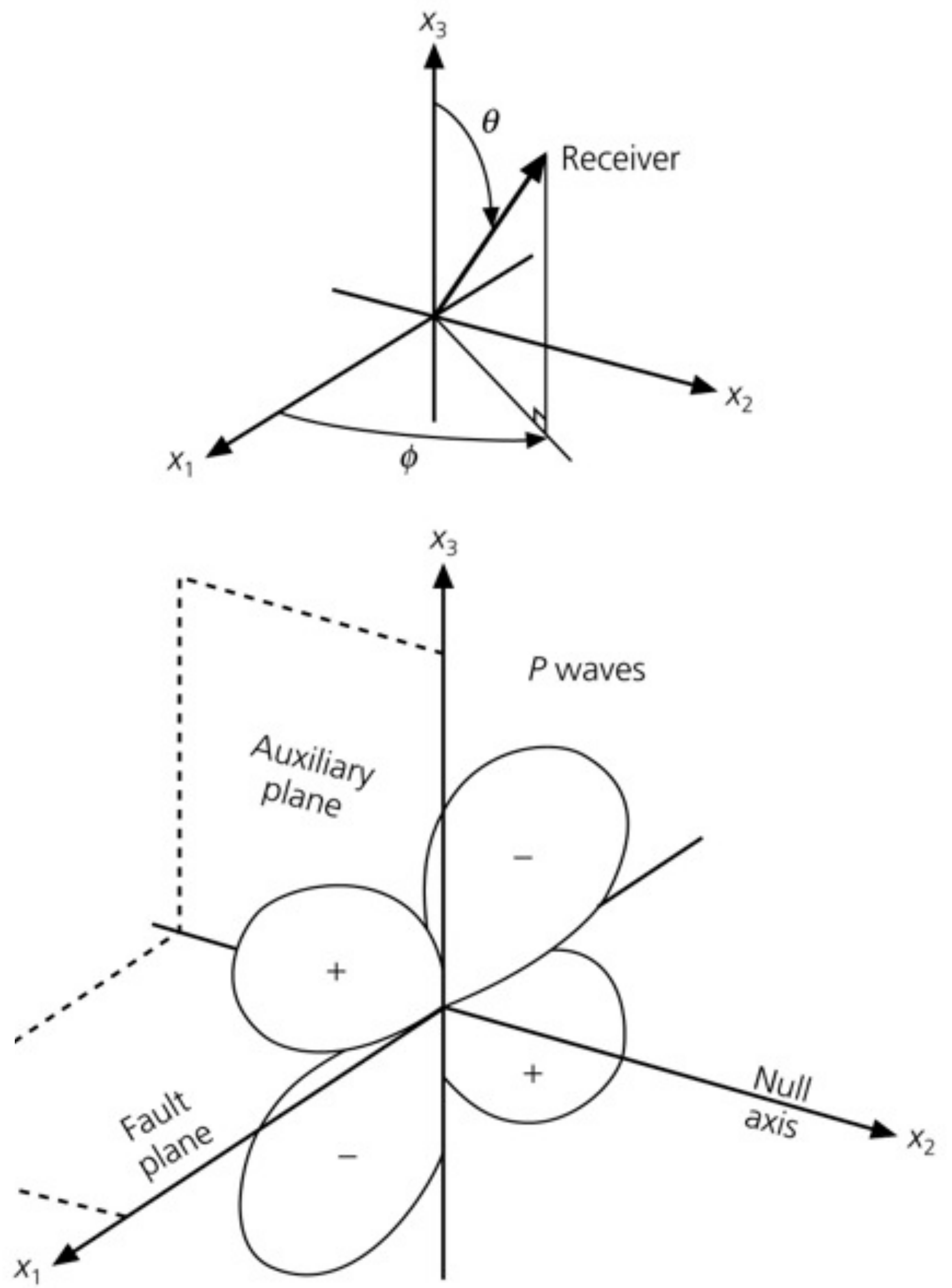

S-wave radiation amplitude patterns:

$$u_\theta = \frac{1}{4\pi\rho\beta^3 r}\ \dot{M}(t - r/\beta)\cos 2\theta \cos\phi$$

$$u_\phi = \frac{1}{4\pi\rho\beta^3 r}\ \dot{M}(t - r/\beta)\,(-\cos\theta \sin\phi)$$

Why are *S* waves usually larger than *P* waves?

These equations predict an average ratio of about α^3/β^3 or about 5.

ıre 4.2-6: Body-wave radiation patterns for a double couple source.

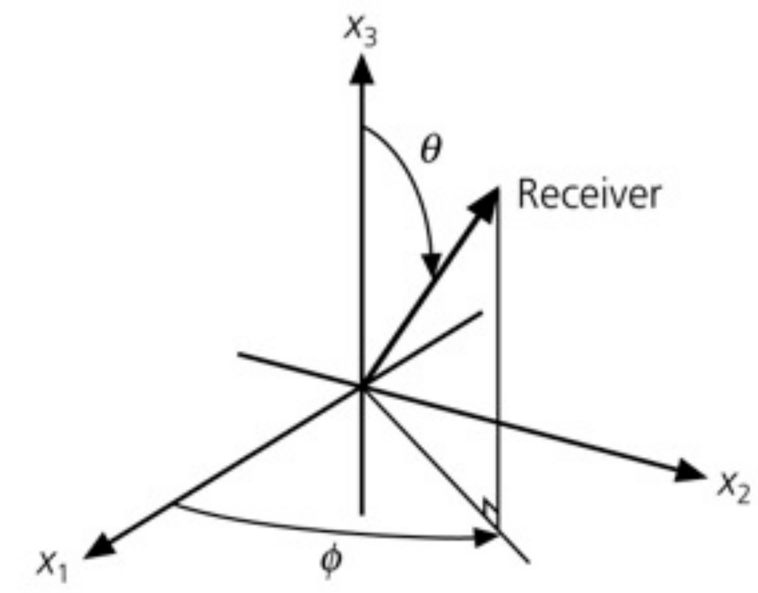

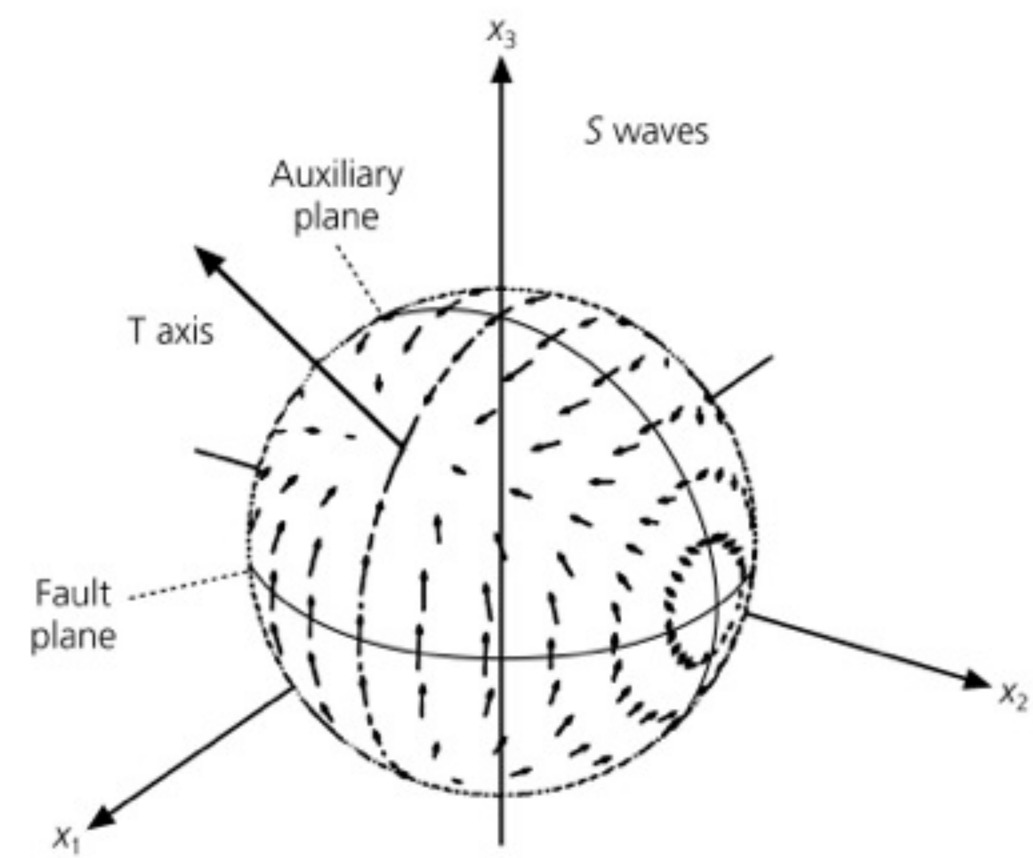

Figure 4.2-7: *P* and *S* radiation amplitude patterns.

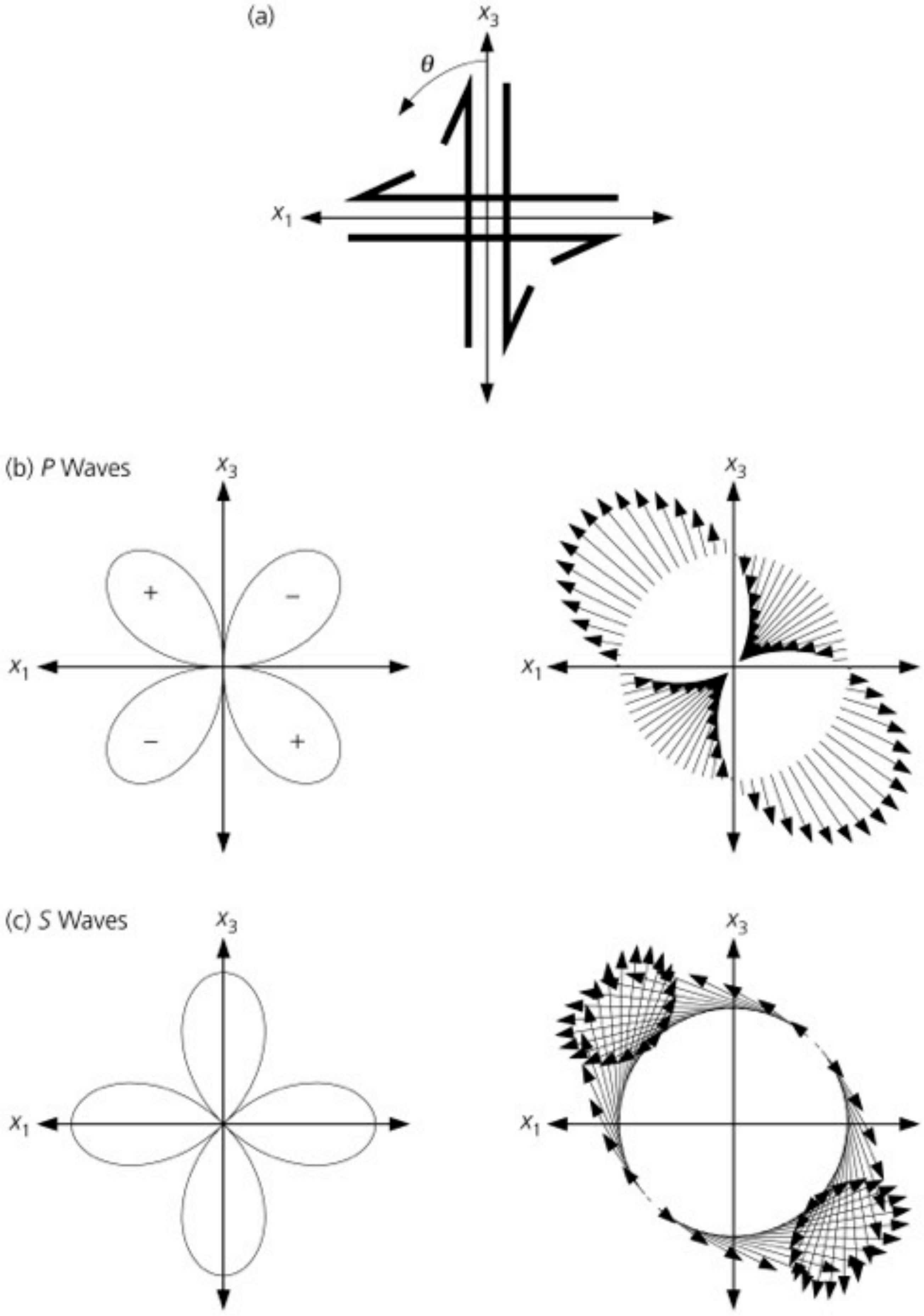

Radiation Patterns in 3D

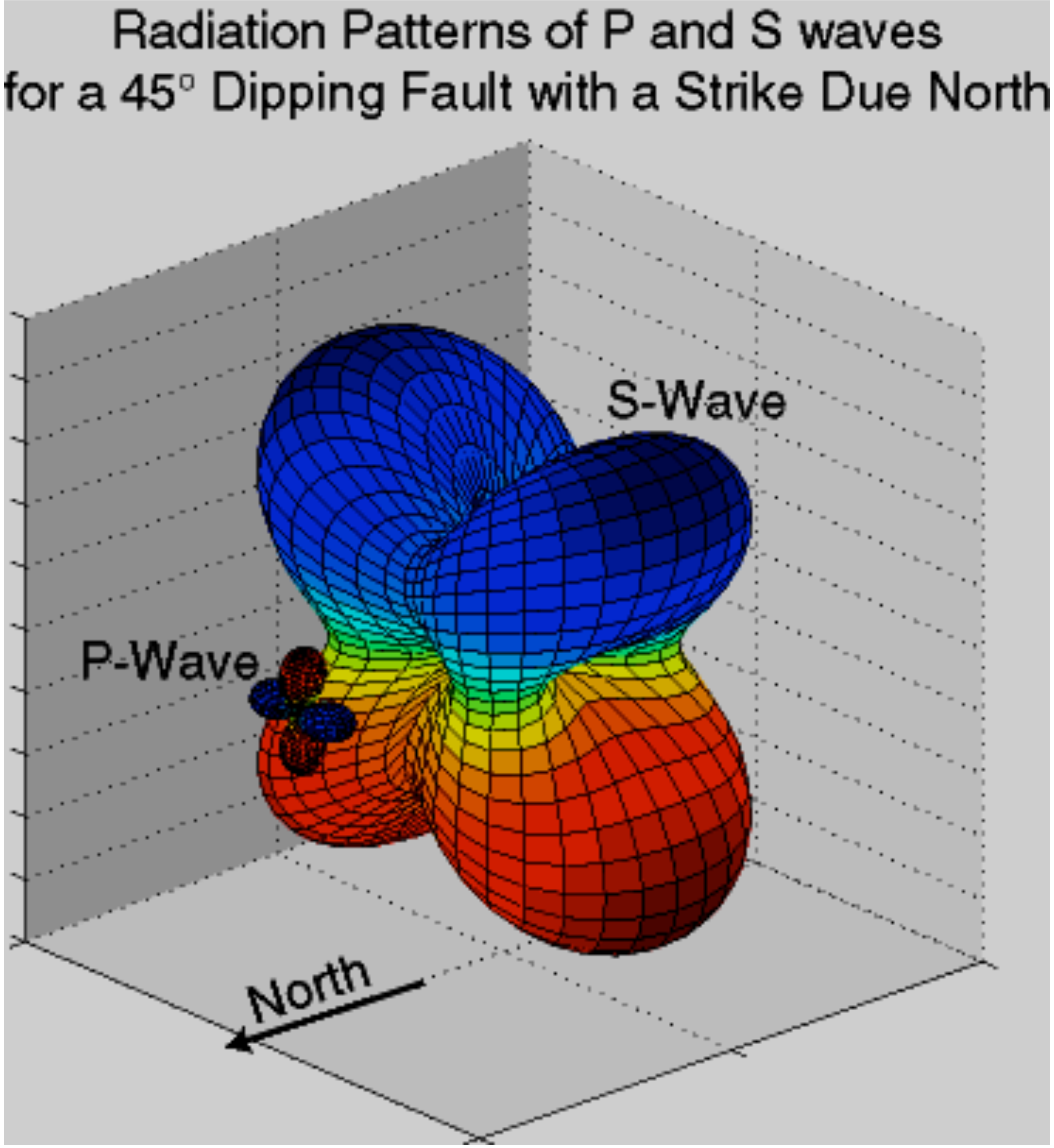

Radiation from shear dislocation

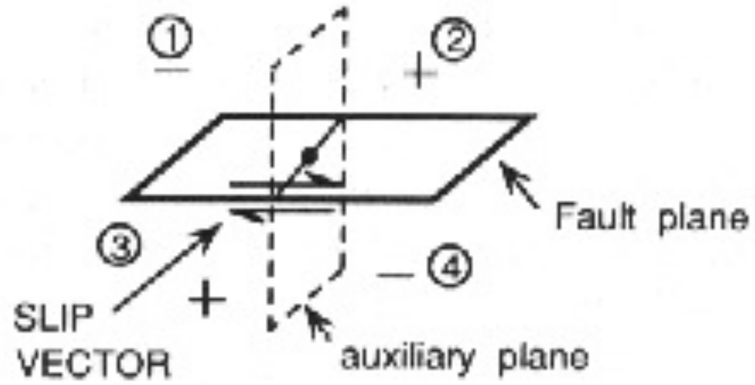

Fault plane and auxiliary plane and sense of initial P-wave motion.

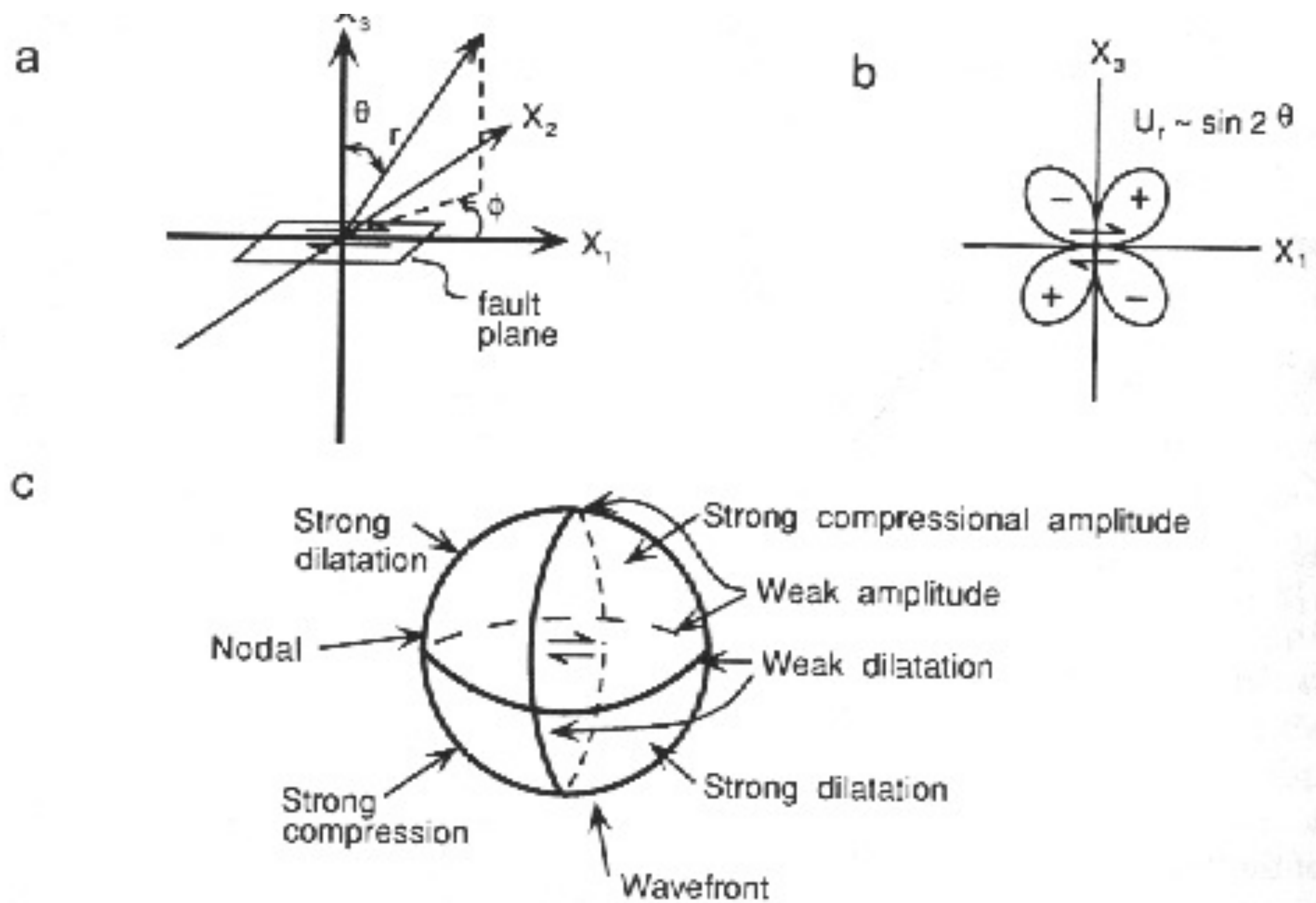

a) Coordinates parallel or perpendicular to fault plane with one axis along the slip direction.

b) radiation pattern in x-z plane

c) 3-D variation of P amplitude and polarity of wavefront from a shear dislocation

Double Couple radiation pattern - P waves

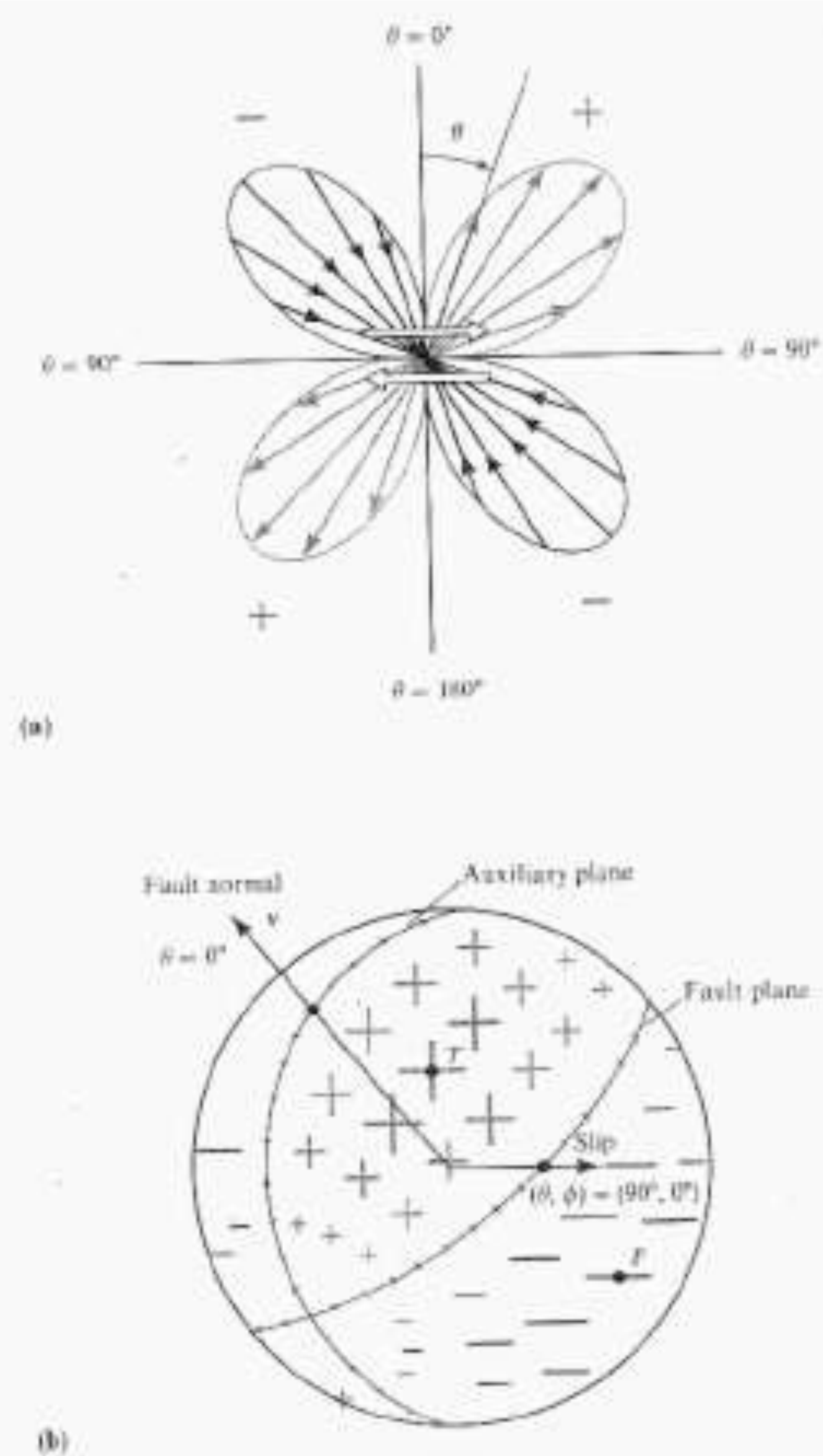

Radiation pattern of the radial displacement component (P-wave) due to a double-couple source:

a) for a plane of constant azimuth (with lobe amplitudes proportional to $\sin 2\theta$). The pair of arrows at the center denotes the shear dislocation.

b) over the focal sphere centered on the origin. Plus and minus signs of various sizes denote amplitude variation (with θ and ϕ) of outward and inward directed motions. The fault plane and auxiliary plane are nodal lines on which $\cos\phi \sin 2\theta = 0$.

Note the alternating quadrants of inward and outward directions.

Double Couple radiation pattern - S waves

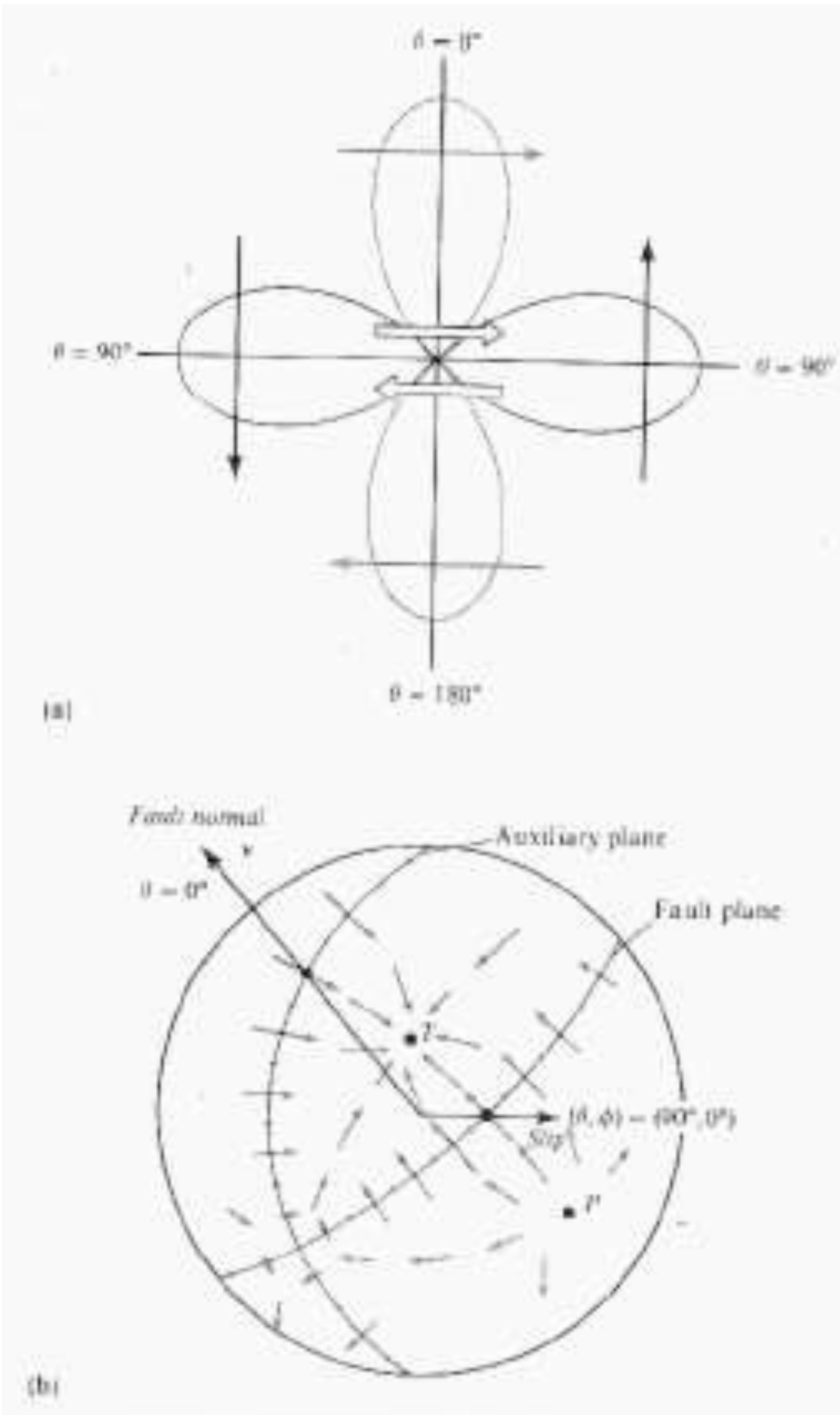

Radiation pattern of the transverse displacement component (S-wave) due to a double-couple source:
a) in the plane { ϕ = 0, $\phi=\pi$ }.
Arrows imposed on each lobe show the direction of particle displacement; the pair of arrows in a) at the center denotes the shear dislocation

b) over a sphere centered on the origin. Arrows with varying size and direction indicate the variation of the transverse motions with θ and ϕ . There are no nodal lines but only nodal points where there is zero motion.
Note that the nodal point for transverse motion at (θ,ϕ) = (45°, 0°) at T is a maximum in the pattern for longitudinal motion while the maximum transverse motion (e.g. at θ = 0) occurs on a nodal line for the longitudinal motion.

Seismic "Beach Balls"

- We use the radiation patterns of P-waves to construct a graphical representation of earthquake faulting geometry.
- The symbols are called "Focal Mechanisms" or "Beach Balls", and they contain information on the fault orientation and the direction of slip.
- They are:
  - Graphical shorthand for a specific faulting process (strike, dip, slip)
  - Projections of a sphere onto a circle (the lower focal hemisphere)
  - Representations of the first motion of seismic waves.
- When mapping the focal sphere to a circle (beachball) two things happen:
  - Lines (vectors) become points
  - Planes become curved lines

Representing a Plane

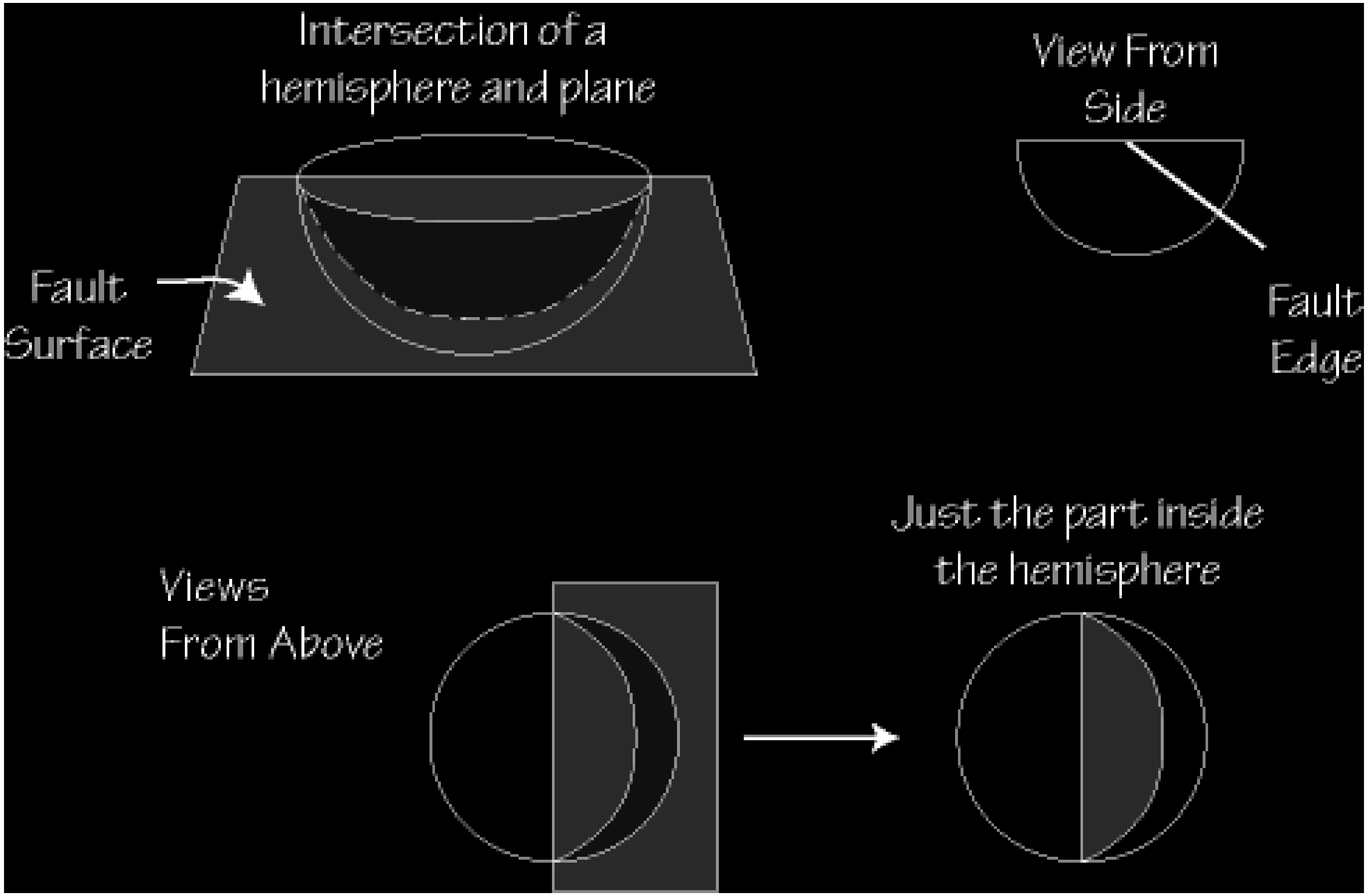

Two steps to understanding

1) The stereographic projection

2) The geometry of first motions and how this is used to define fault motion.

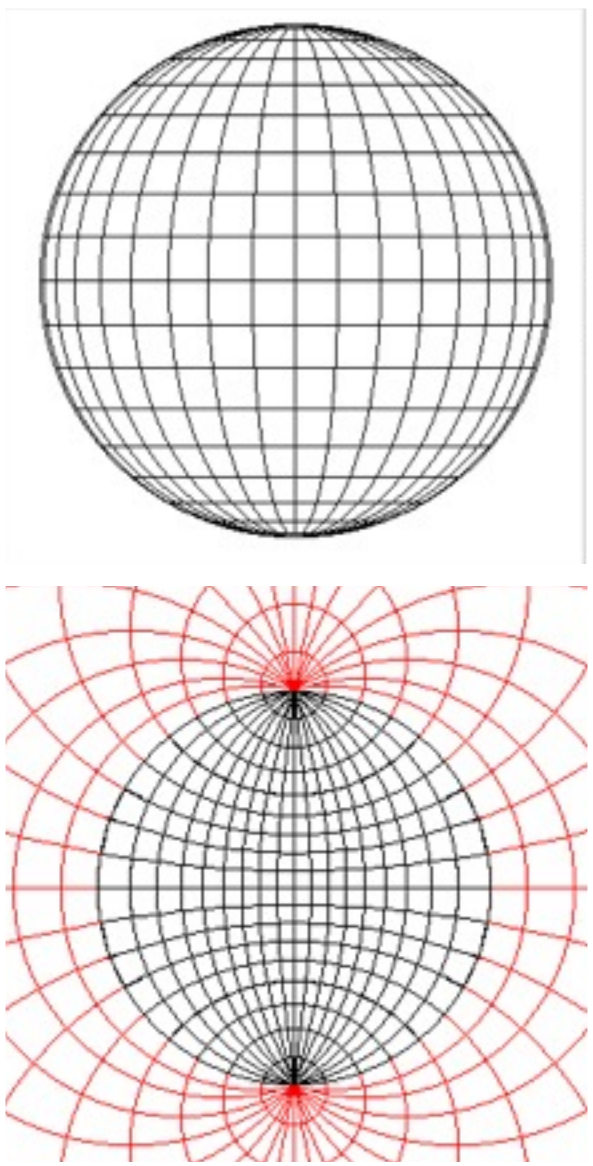

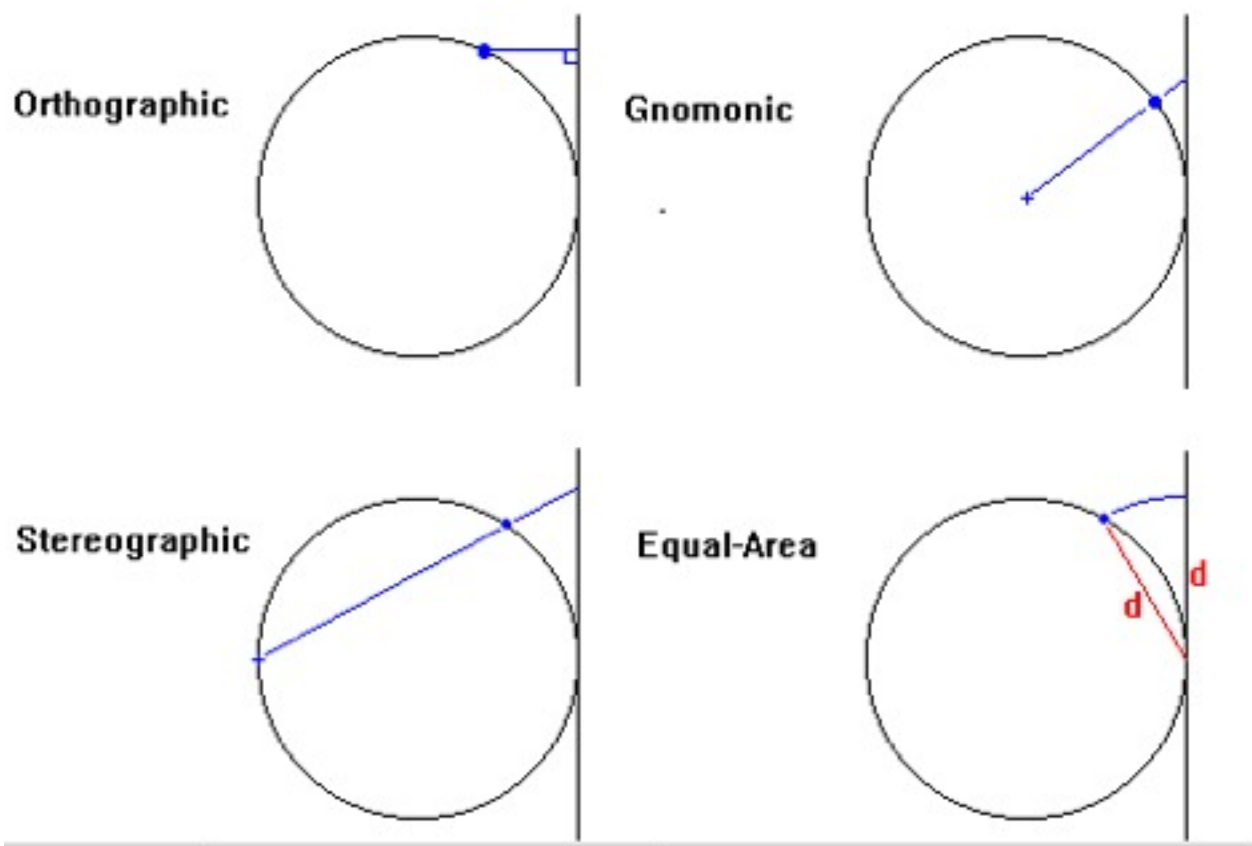

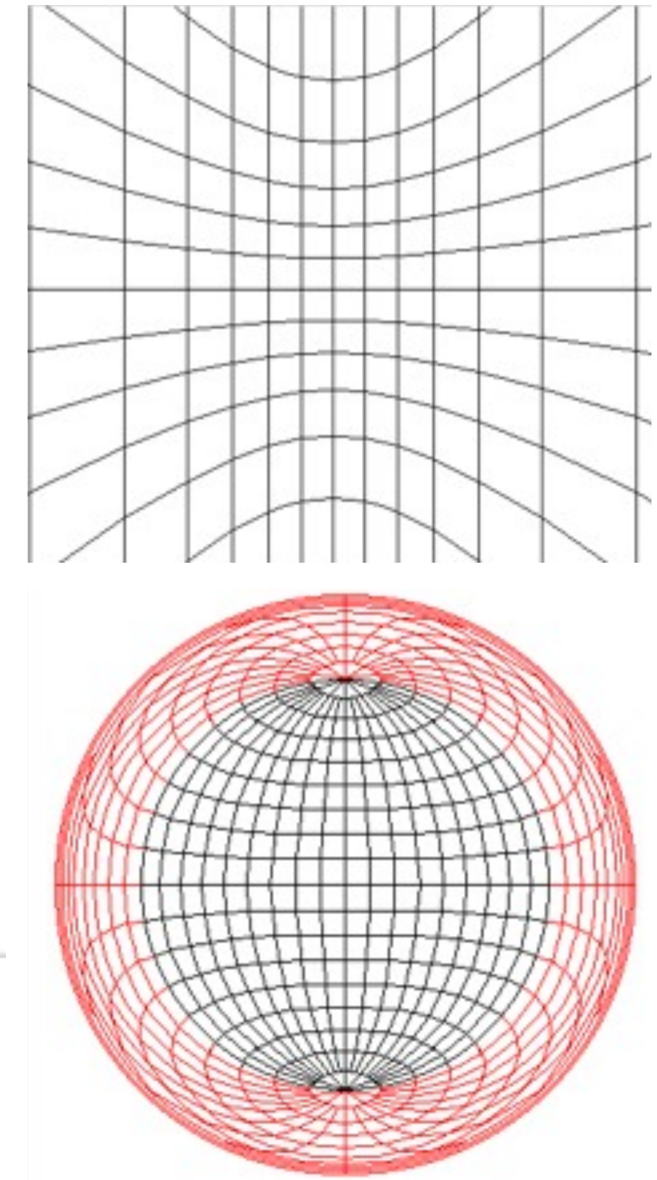

Source:USGS

http://www.uwsp.edu/geo/projects/geoweb/participants/dutch/STRUCTGE/sphproj.htm

Stereonets

- A template called a stereonet is used to plot data.
- Example – plotting planes (e.g. faults)

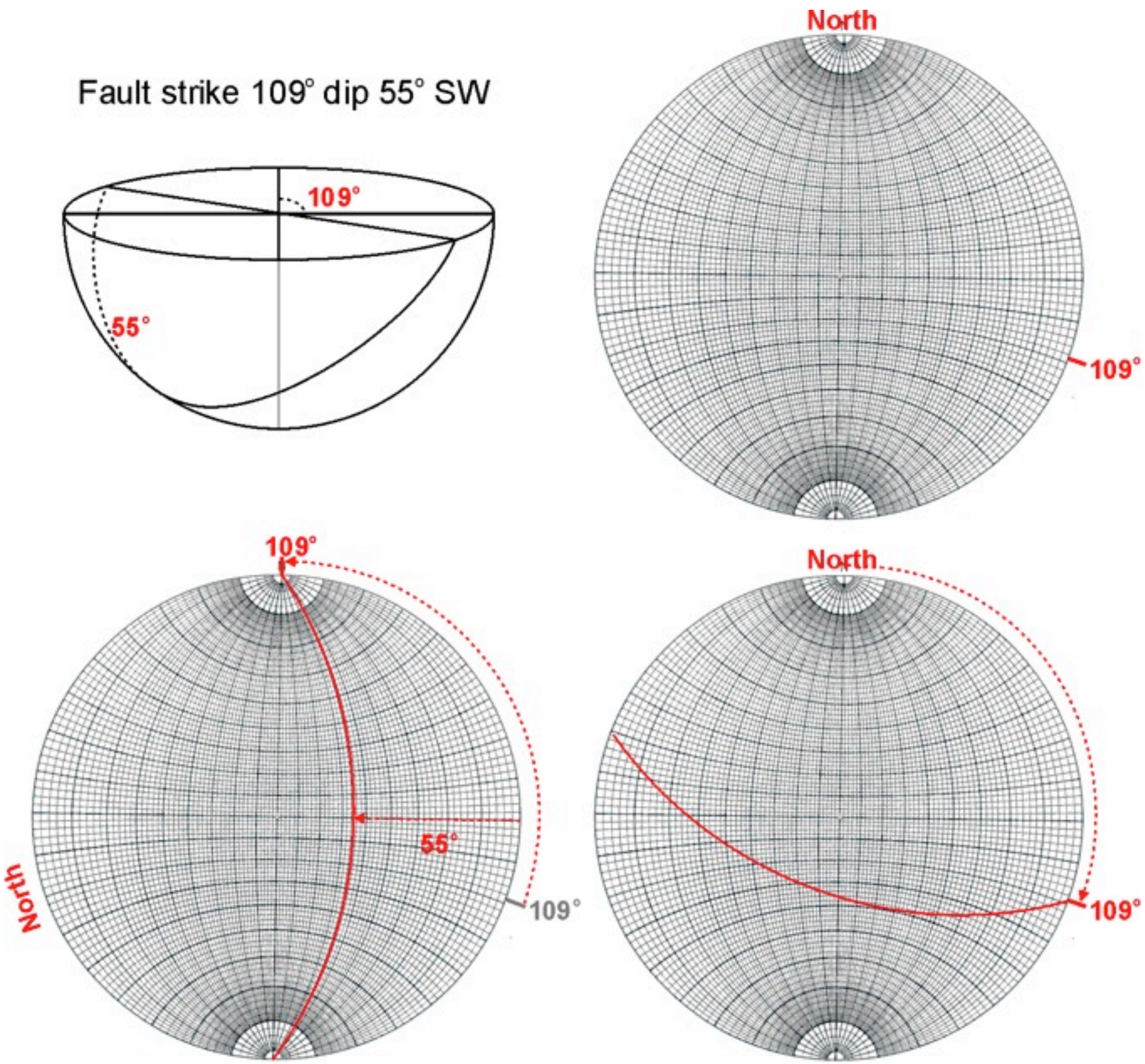

Source:USGS

- Example – plotting lines (e.g. ray paths)

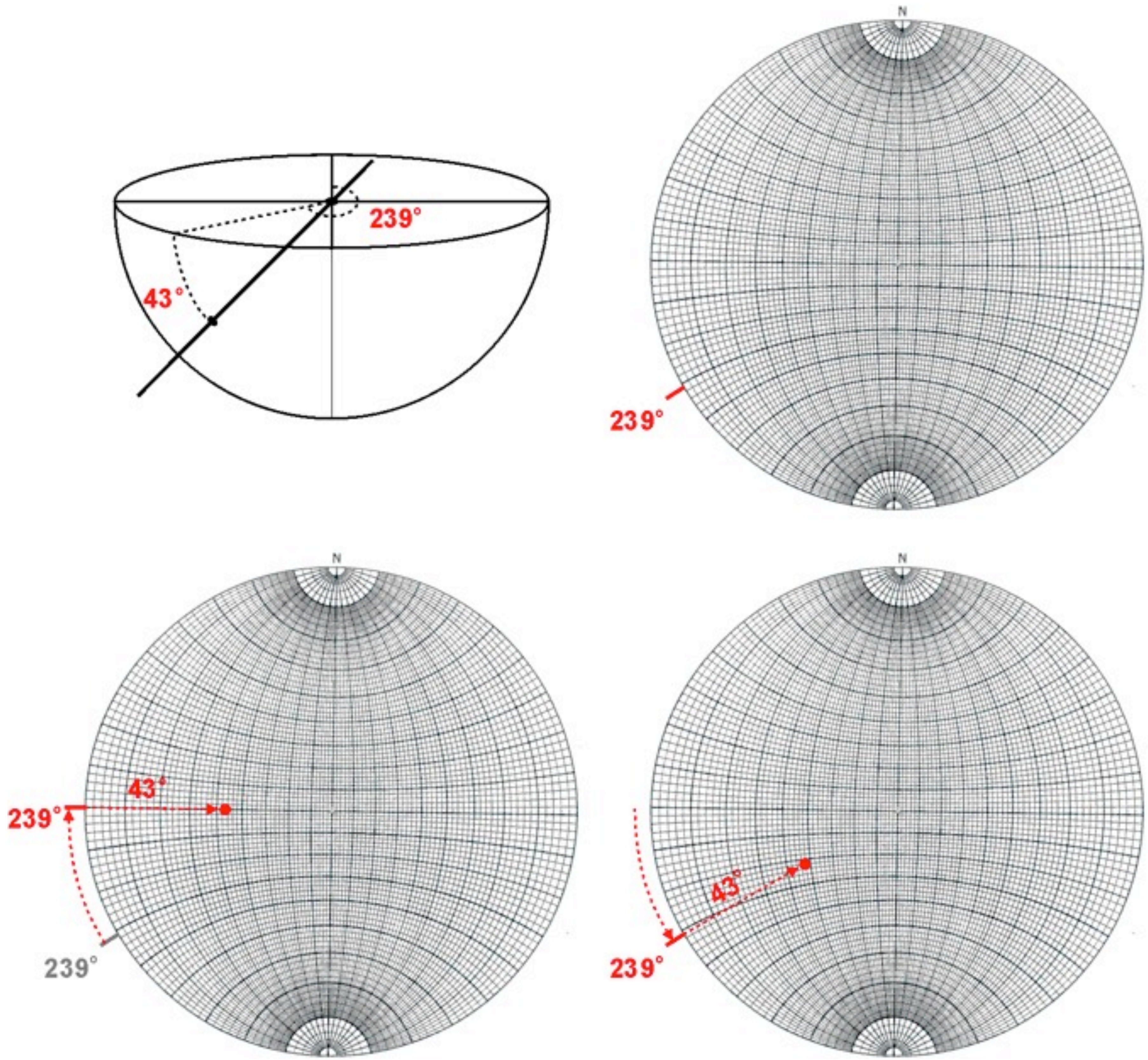

Source:USGS

Stereonets

- Example – pitch (or rake) of a line on a plane (e.g. the slip direction on a fault)

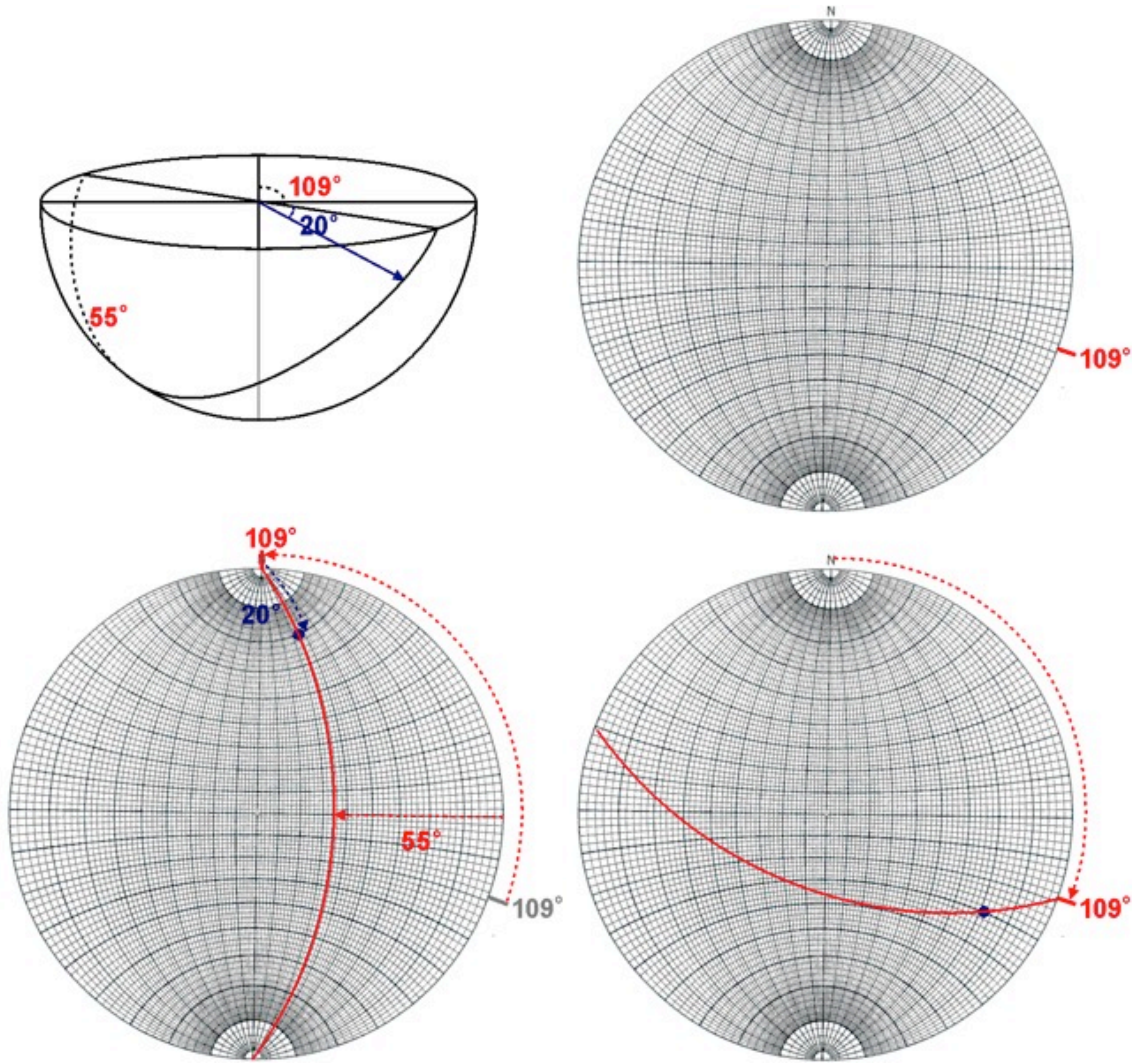

Source:USGS

Focal sphere

In order to simplify the analysis, the concept of the "focal sphere" is introduced. The focal sphere is an imaginary sphere drawn around the source region enclosing the fault. If we know the earthquake location and local Earth structure, we can trace rays from the source region to the stations and find the ray take-off angle at the source to a given station.

Figure 4.2-8: Cartoon of the focal sphere.

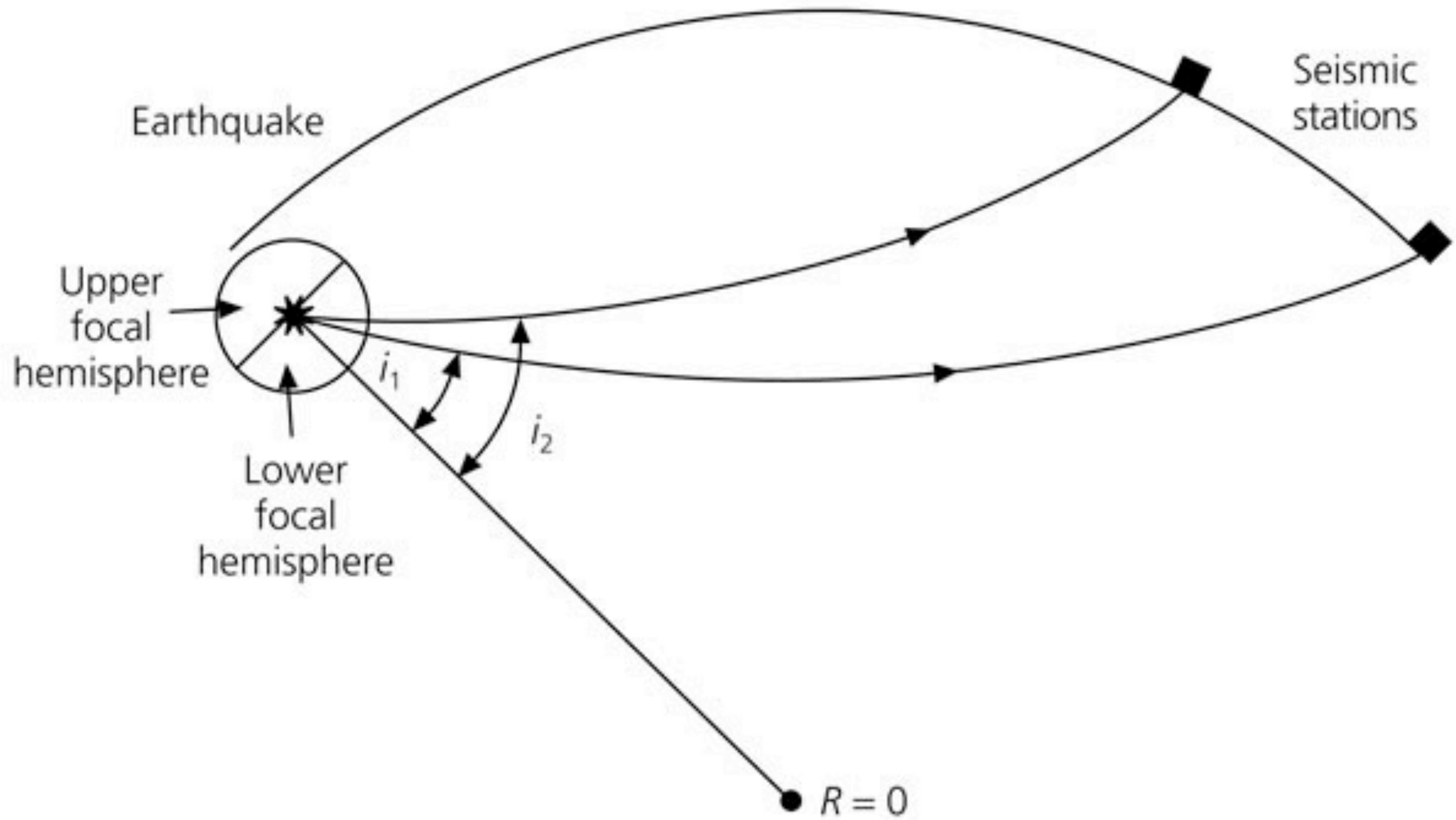

Take-off angle

At a given source-receiver, the distance can be determined and from this T and the slope (p) can be found from the travel time tables. For example, the Jeffreys-Bullen travel time tables can be used to obtain p and from this the take-off angle i.

Table 4.2-1: ***P*** **wave take-off angles for a surface focus earthquake.**

Distance (°)	Take-off angle (°)	Distance (°)	Take-off angle (°)	Distance (°)	Take-off angle (°)
21	35	47	25	73	19
23	32	49	24	75	18
25	30	51	24	77	18
27	29	53	23	79	17
29	29	55	23	81	17
31	29	57	23	83	16
33	28	59	22	85	16
35	28	61	22	87	15
37	27	63	21	89	15
39	29	65	21	91	15
41	26	67	20	93	14
43	26	69	20	95	14
45	25	71	19	97	14

Radiation from shear dislocation

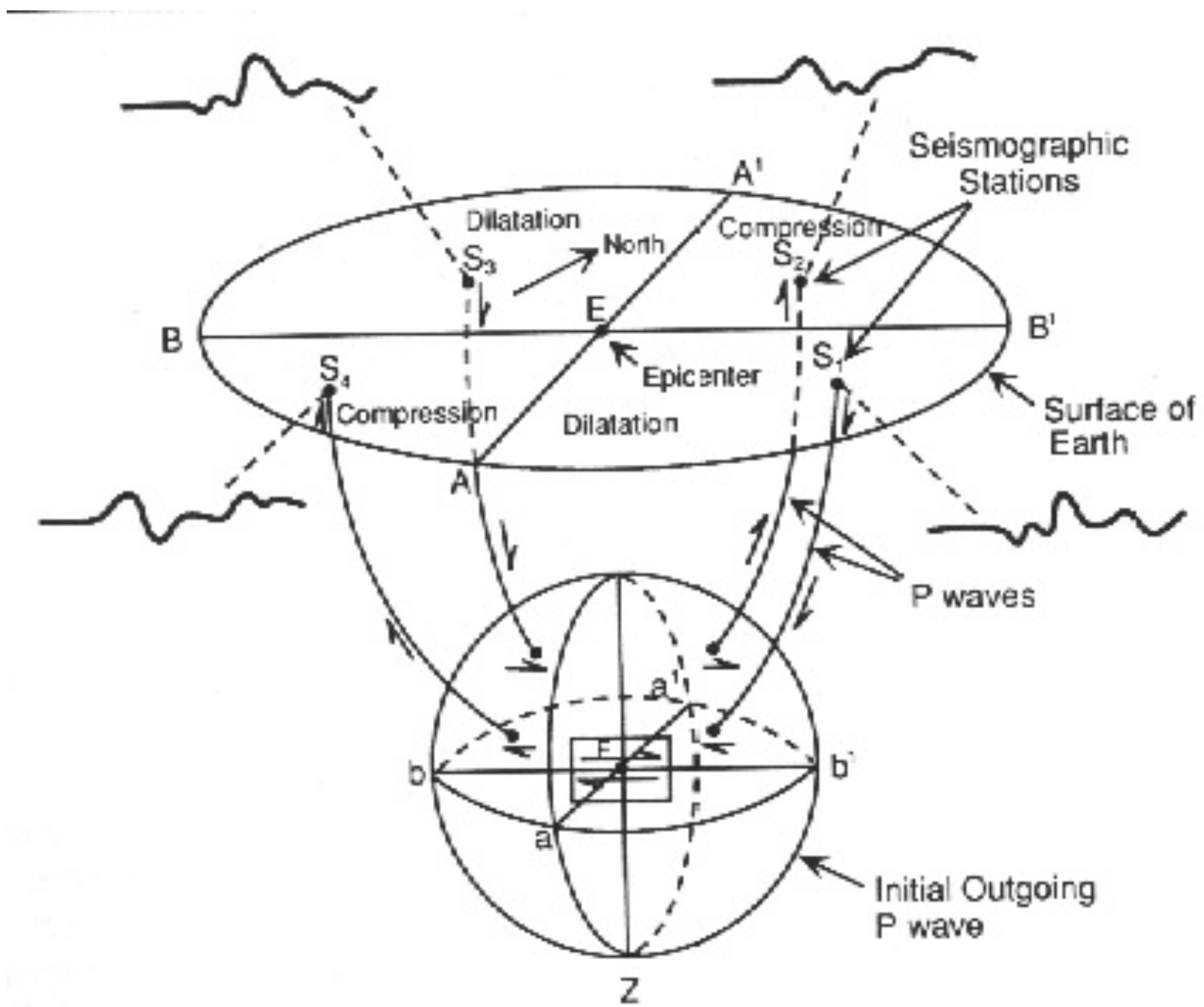

First motion of P waves at seismometers in various directions.

The polarities of the observed motion is used to determine the point source characteristics.

Beachballs always have two curved lines separating the quadrants, i.e. they show two planes. But there is only one fault plane and the other is called the auxiliary plane. Seismologists cannot tell which is which from seismograms alone, so we always show both of the possible solutions.

Manual determination of focal mechanism

To obtain a fault plane solution basically three steps are required:

1. Calculating the positions of the penetration points of the seismic rays through the focal sphere which are defined by the ray azimuth and the take-off angle of the ray from the source.
2. Marking these penetration points through the upper or lower hemisphere in a horizontal (stereographic) projection sphere using different symbols for compressional and dilatational first arrivals.
3. Partitioning the projection of the lower focal sphere by two perpendicular great circles which separate all (or at least most) of the + and - arrivals in different quadrants.

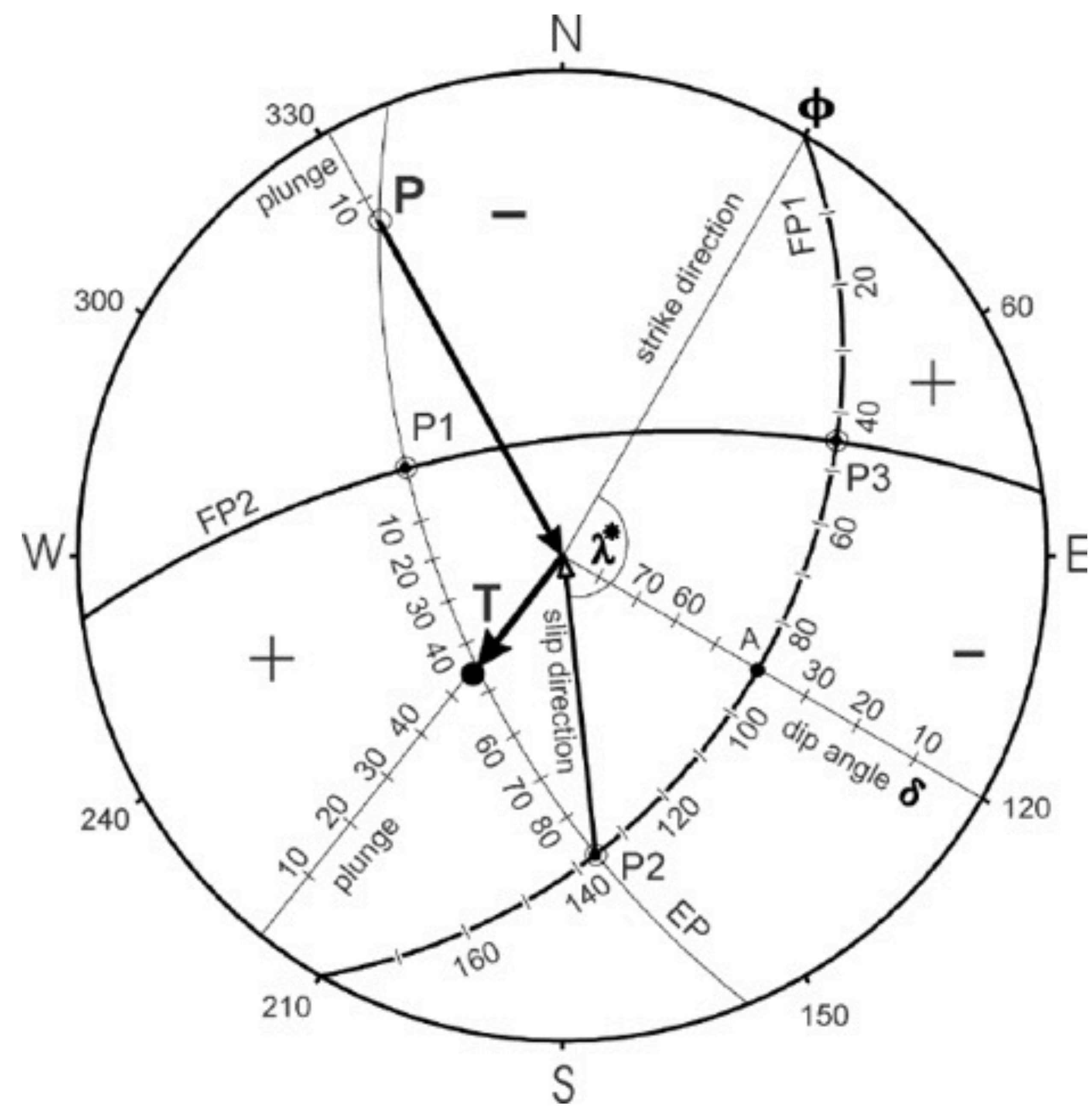

P1, P2 and P3 mark the positions of the poles of the planes FP1 (fault plane), FP2 (auxiliary plane) and EP (equatorial plane) in their net projections. On the basis of polarity readings alone it can not be decided whether FP1 or FP2 was the really acting fault. A discrimination requires additionally studies

Fault types and focal mechanisms

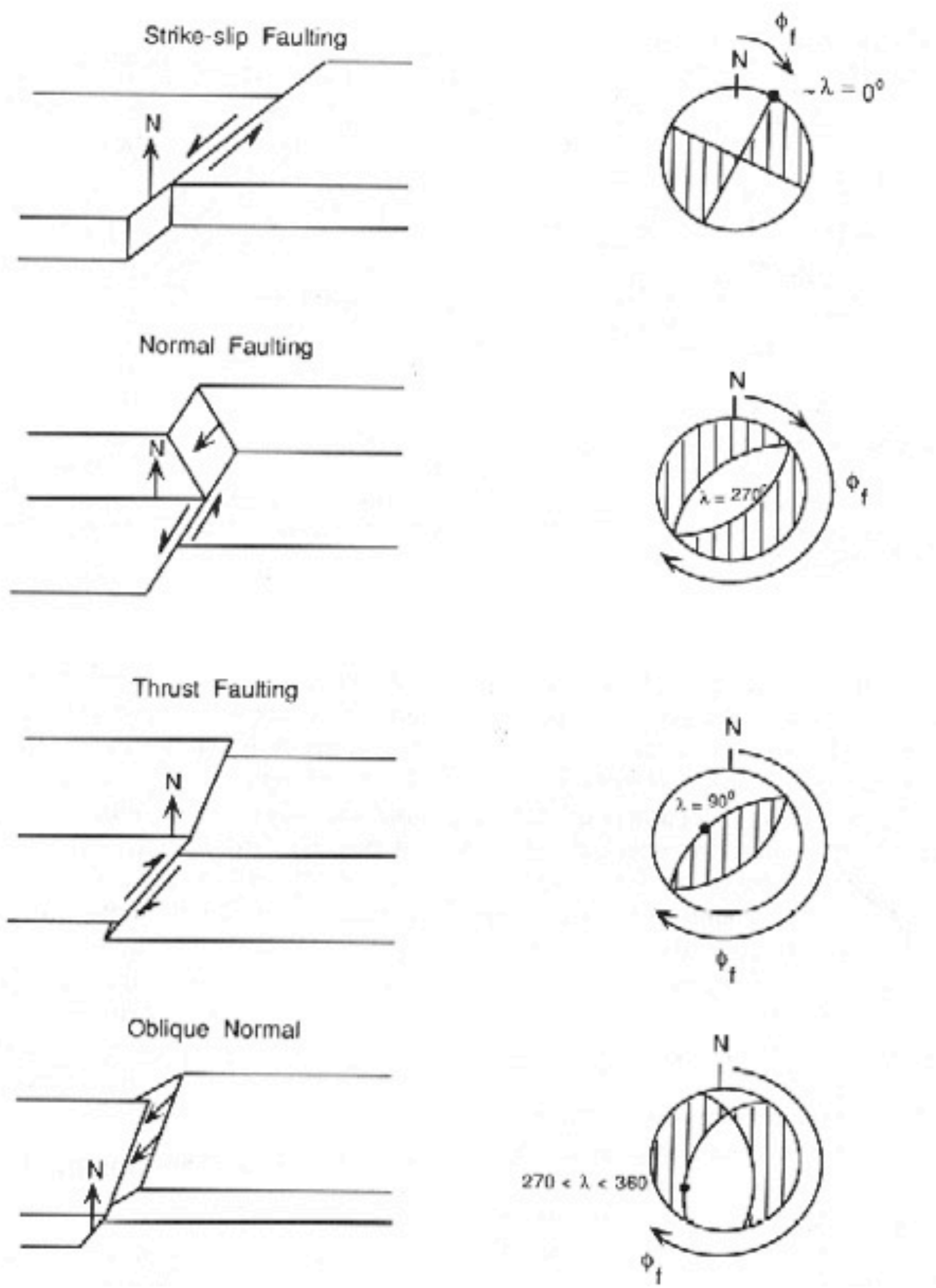

Basis fault types and their appearance in the focal mechanisms. Dark regions indicate compressional P-wave motion.

The Principal Mechanisms

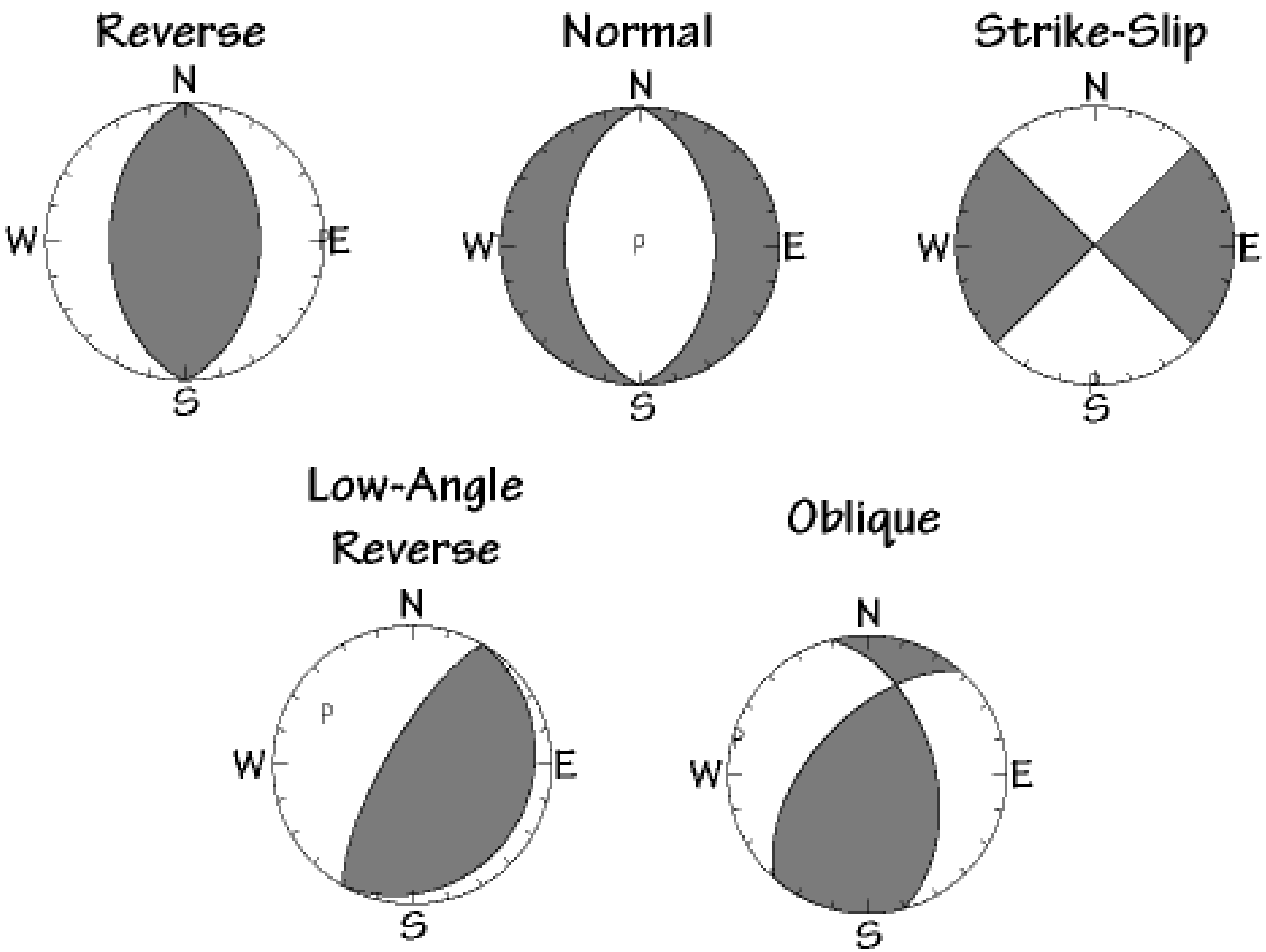

FM & stress axes

Figure 4.2-16: Relation between fault planes and stress axes.

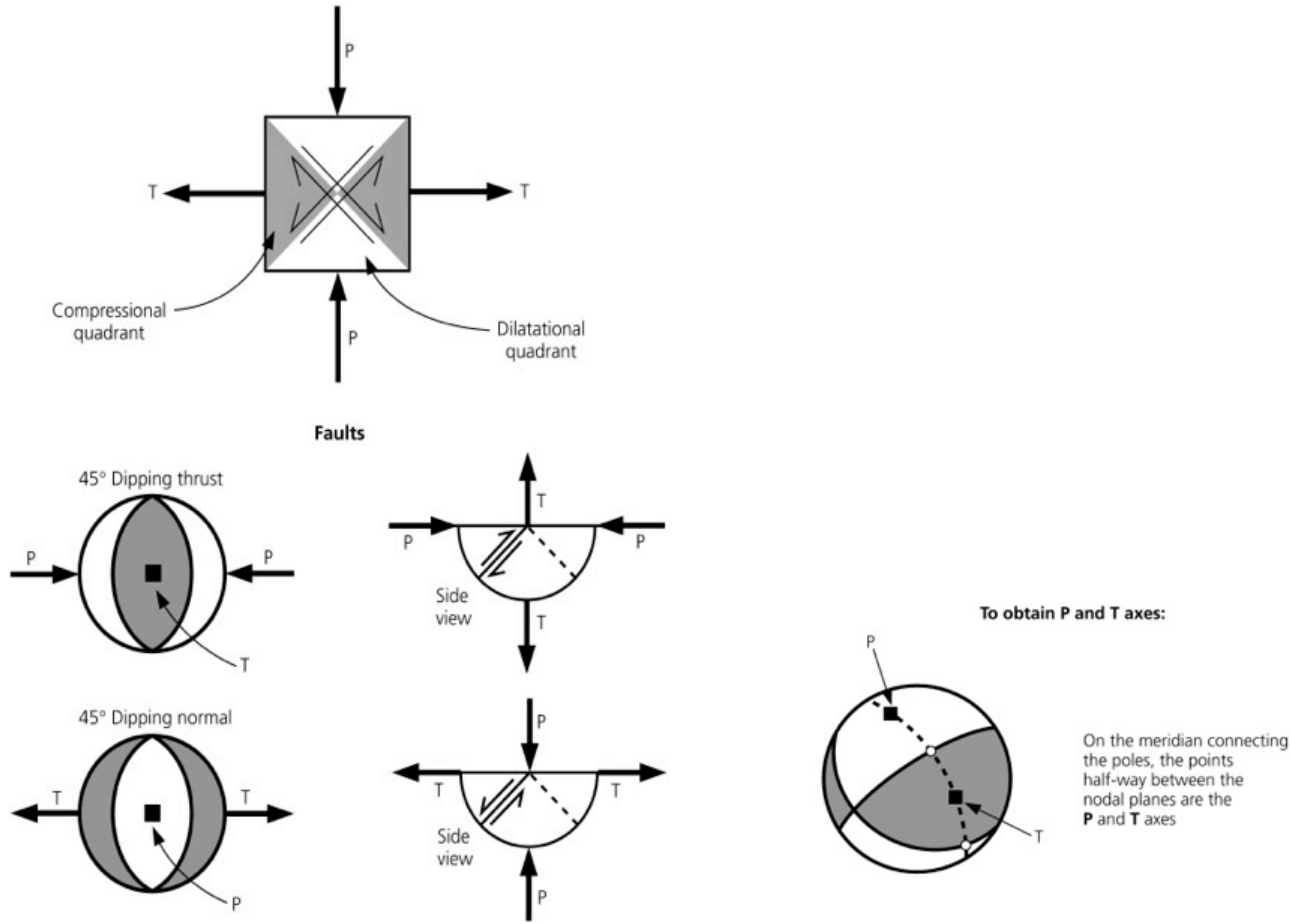

Figure 4.2-17: Examples of focal mechanisms and first motions.

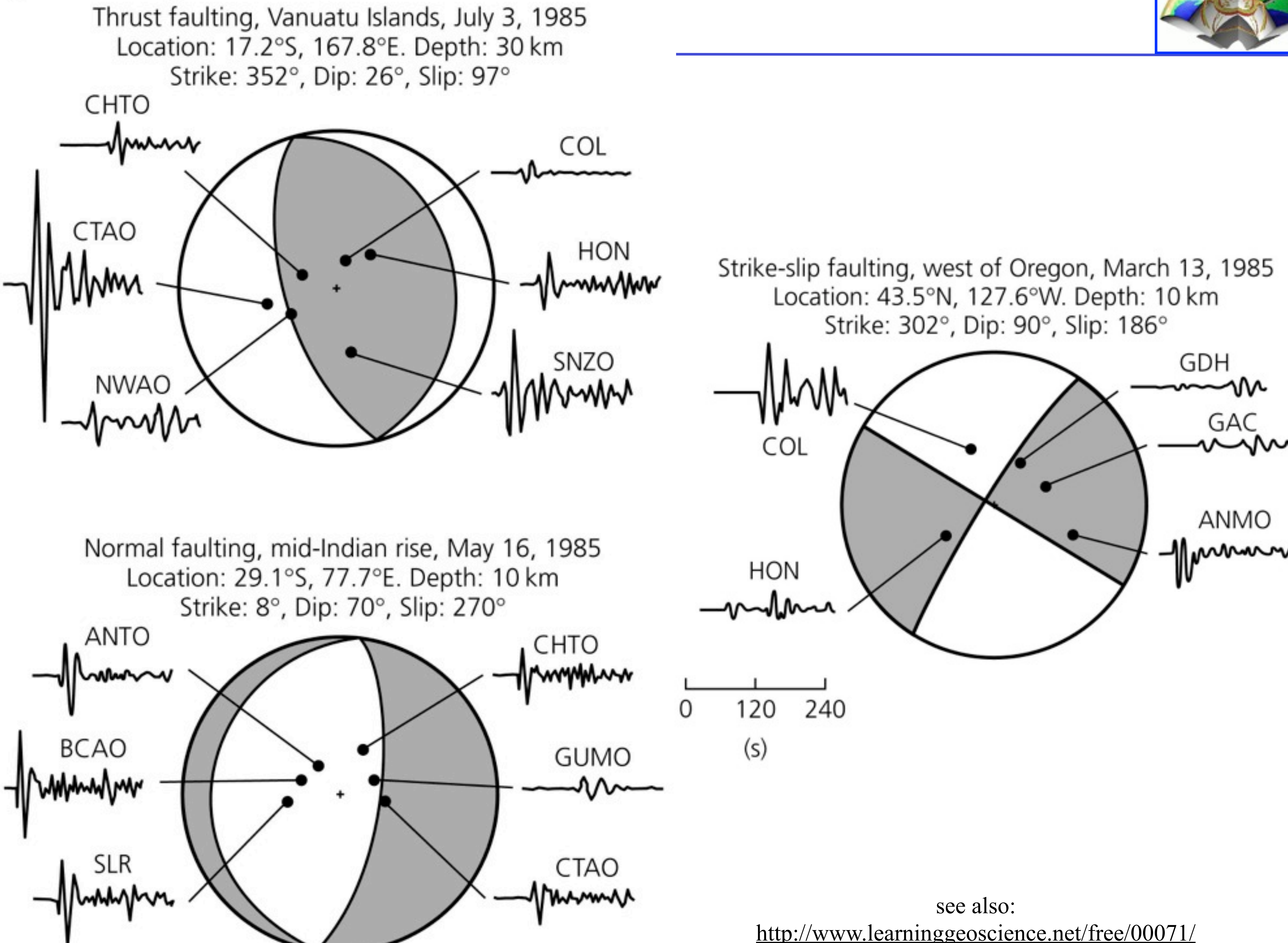

see also:
http://www.learninggeoscience.net/free/00071/

Double couple RP & surface waves

Figure 4.3-12: Surface wave amplitude radiation patterns for several focal mechanisms.

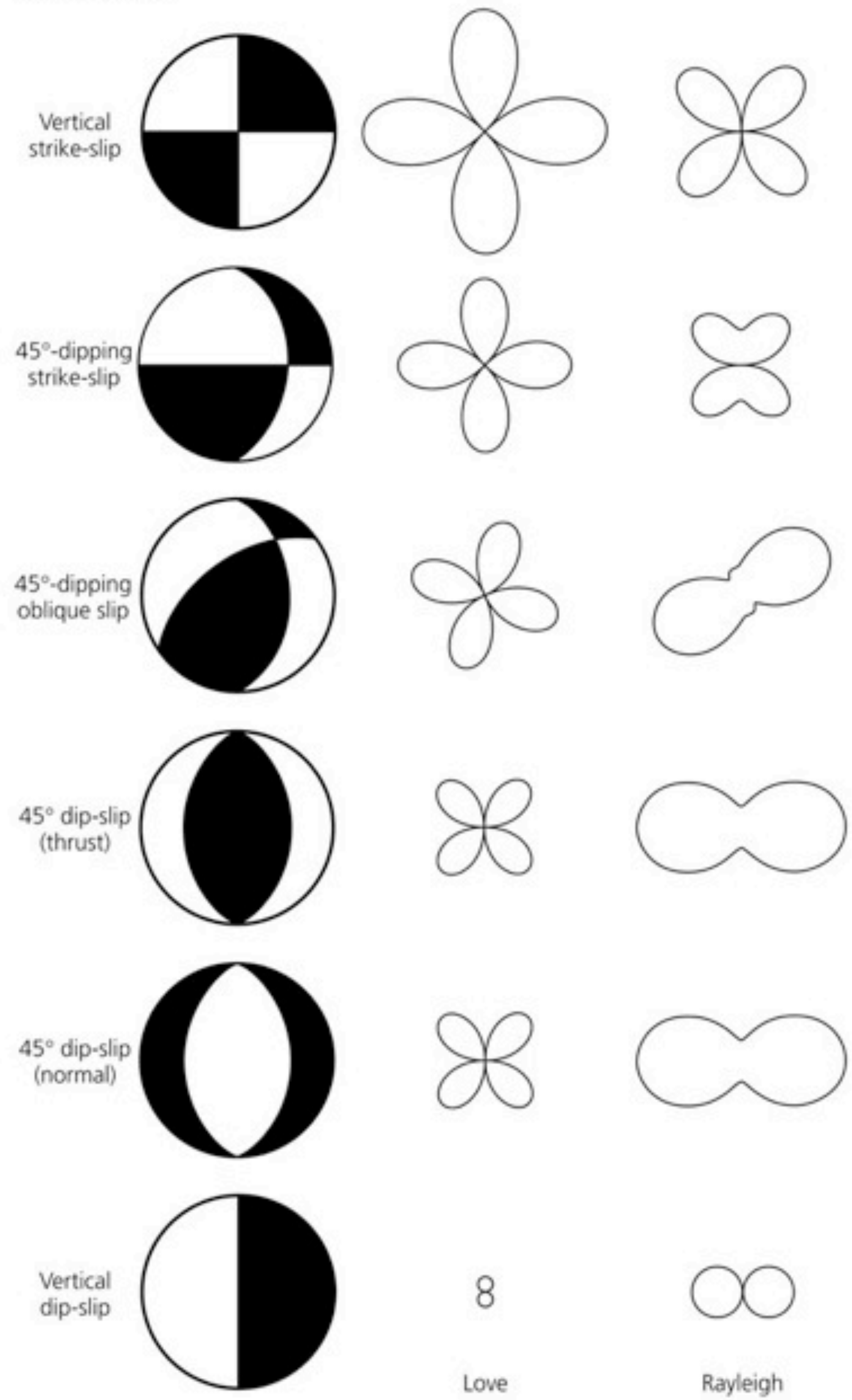

FM & Moment tensor

Figure 4.4-6: Selected moment tensors and their associated focal mechanisms.

Moment tensor	Beachball	Moment tensor	Beachball
$\frac{1}{\sqrt{3}}\begin{pmatrix}1&0&0\\0&1&0\\0&0&1\end{pmatrix}$		$-\frac{1}{\sqrt{3}}\begin{pmatrix}1&0&0\\0&1&0\\0&0&1\end{pmatrix}$	
$-\frac{1}{\sqrt{2}}\begin{pmatrix}0&1&0\\1&0&0\\0&0&0\end{pmatrix}$		$\frac{1}{\sqrt{2}}\begin{pmatrix}1&0&0\\0&-1&0\\0&0&0\end{pmatrix}$	
$\frac{1}{\sqrt{2}}\begin{pmatrix}0&0&-1\\0&0&0\\-1&0&0\end{pmatrix}$		$\frac{1}{\sqrt{2}}\begin{pmatrix}0&0&0\\0&0&-1\\0&-1&0\end{pmatrix}$	
$\frac{1}{\sqrt{2}}\begin{pmatrix}-1&0&0\\0&0&0\\0&0&1\end{pmatrix}$		$\frac{1}{\sqrt{2}}\begin{pmatrix}0&0&0\\0&-1&0\\0&0&1\end{pmatrix}$	
$\frac{1}{\sqrt{6}}\begin{pmatrix}1&0&0\\0&-2&0\\0&0&1\end{pmatrix}$		$\frac{1}{\sqrt{6}}\begin{pmatrix}-2&0&0\\0&1&0\\0&0&1\end{pmatrix}$	
$\frac{1}{\sqrt{6}}\begin{pmatrix}1&0&0\\0&1&0\\0&0&-2\end{pmatrix}$		$-\frac{1}{\sqrt{6}}\begin{pmatrix}1&0&0\\0&1&0\\0&0&-2\end{pmatrix}$	

Faults and Plates

The style of faulting tells us something about the forces acting in a particular part of Earth.

Along plate boundaries, faulting reflects the motion of plates.

- Divergent Boundary = Normal Faulting
- Convergent Boundary = Reverse Faulting
- Transform Boundary = Strike-Slip Faulting

Where are the Normal Faults?

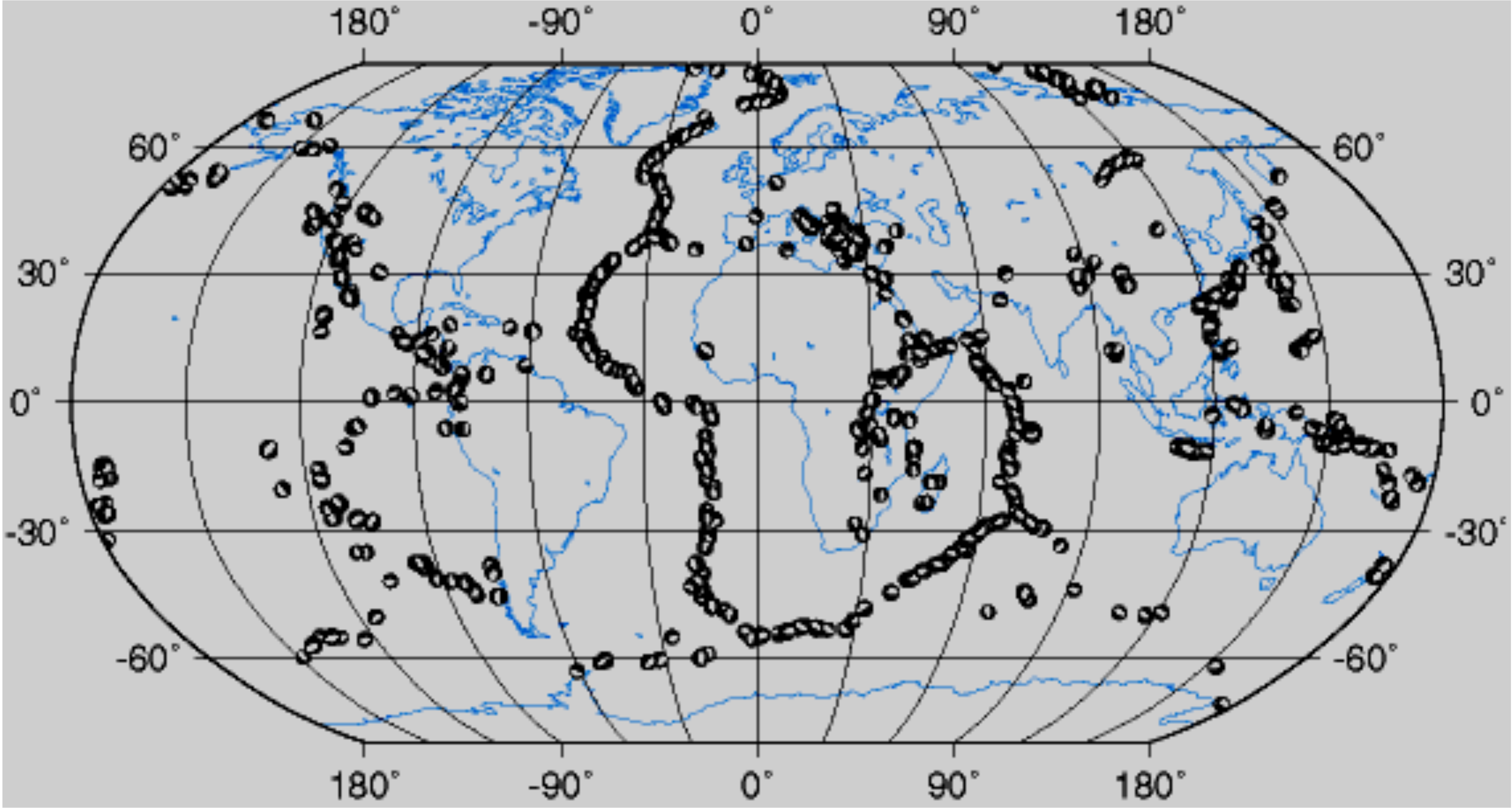

Where are the Reverse Faults?

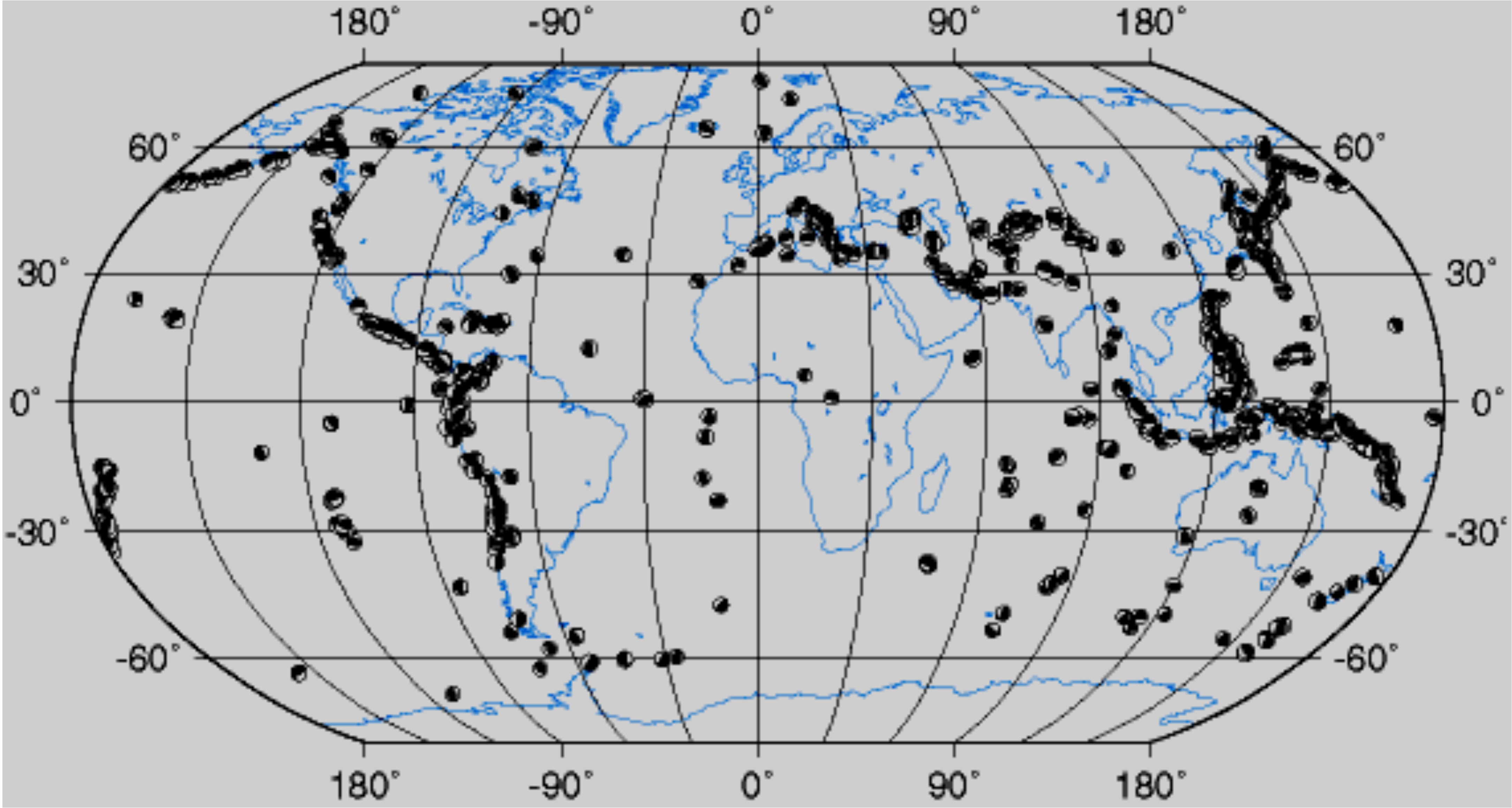

Where are the Transform Faults?

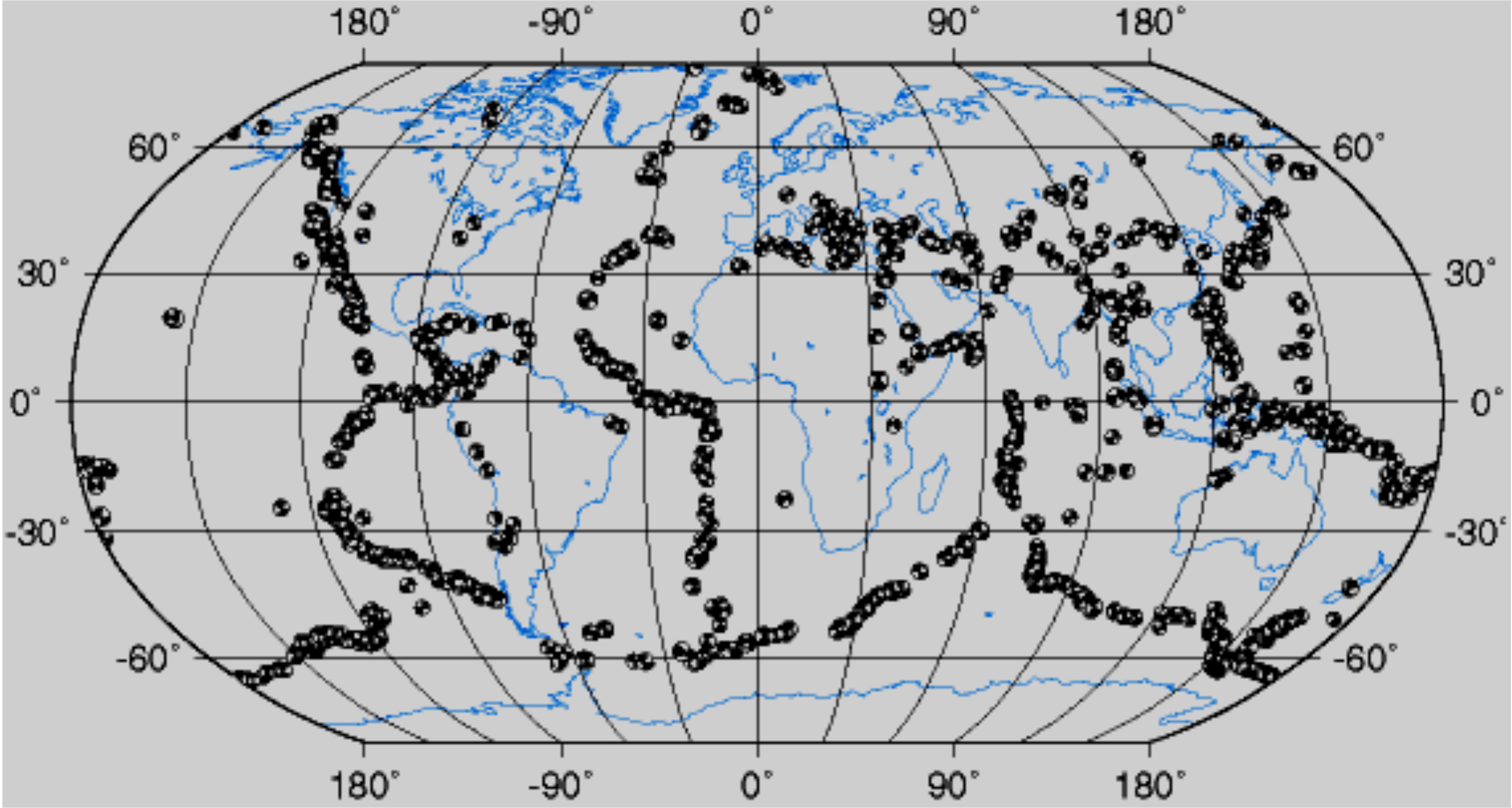

Example: East Africa

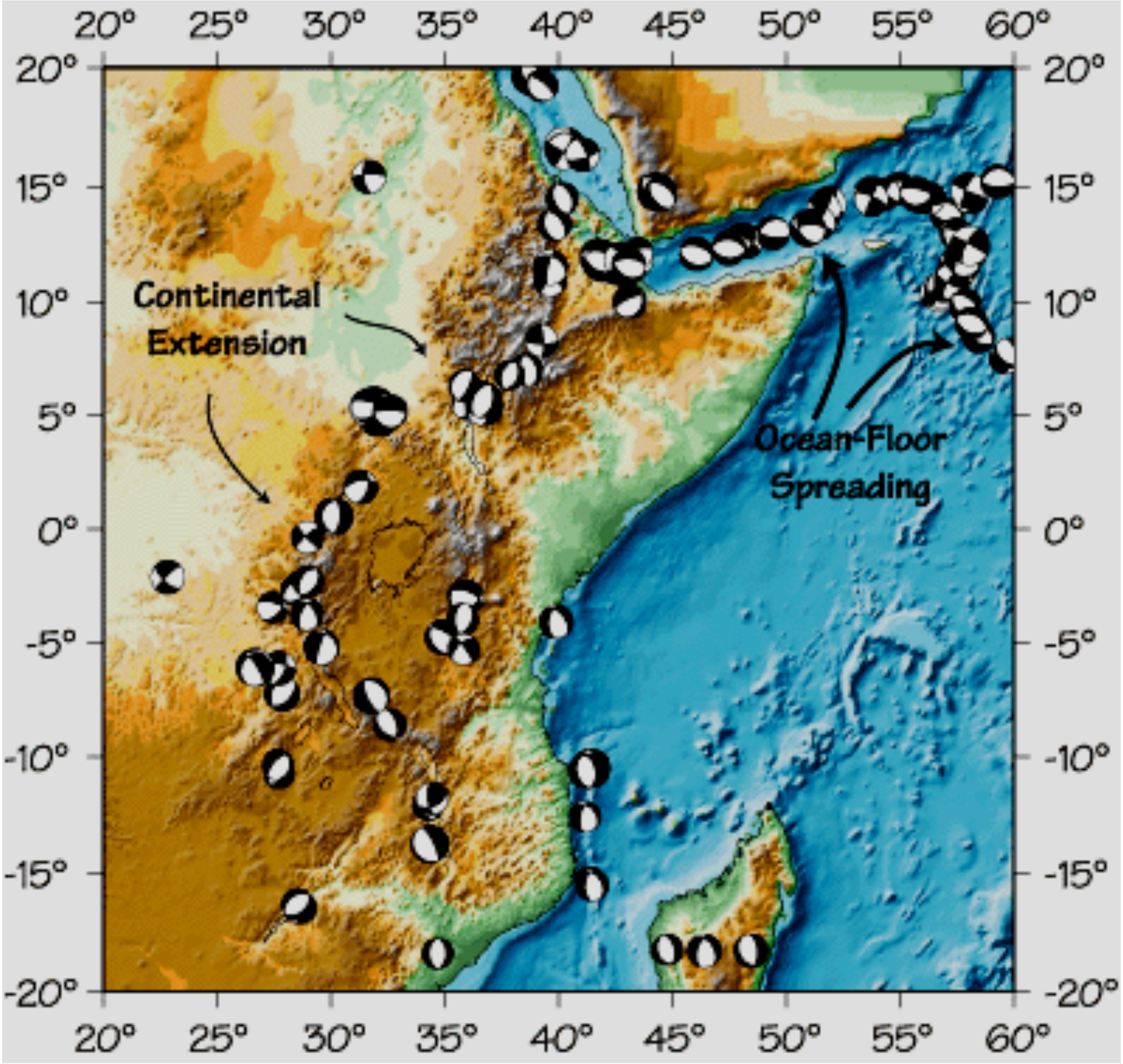

Faulting

- So far we have talked about the faulting of shallow earthquakes, which are well explained by plate tectonics.

- What about the faulting style of deep earthquakes ?

- Do similar principles hold true?

Faulting

- We sometimes see "normal" faulting at depths of 100 km or so in subduction zones:

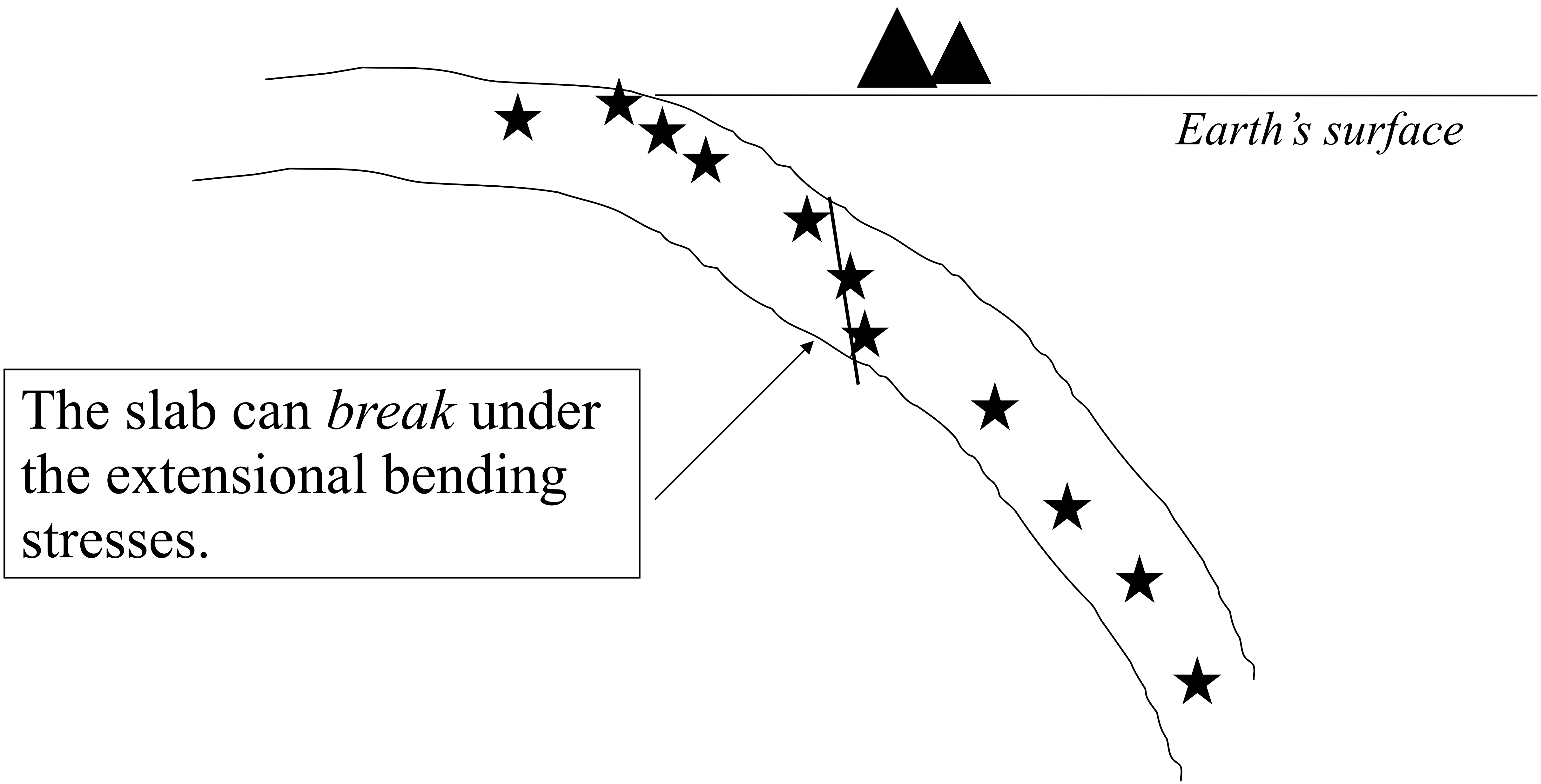

Faulting

- We sometimes see "reverse" faulting for the deepest earthquakes at about 600 km depth:

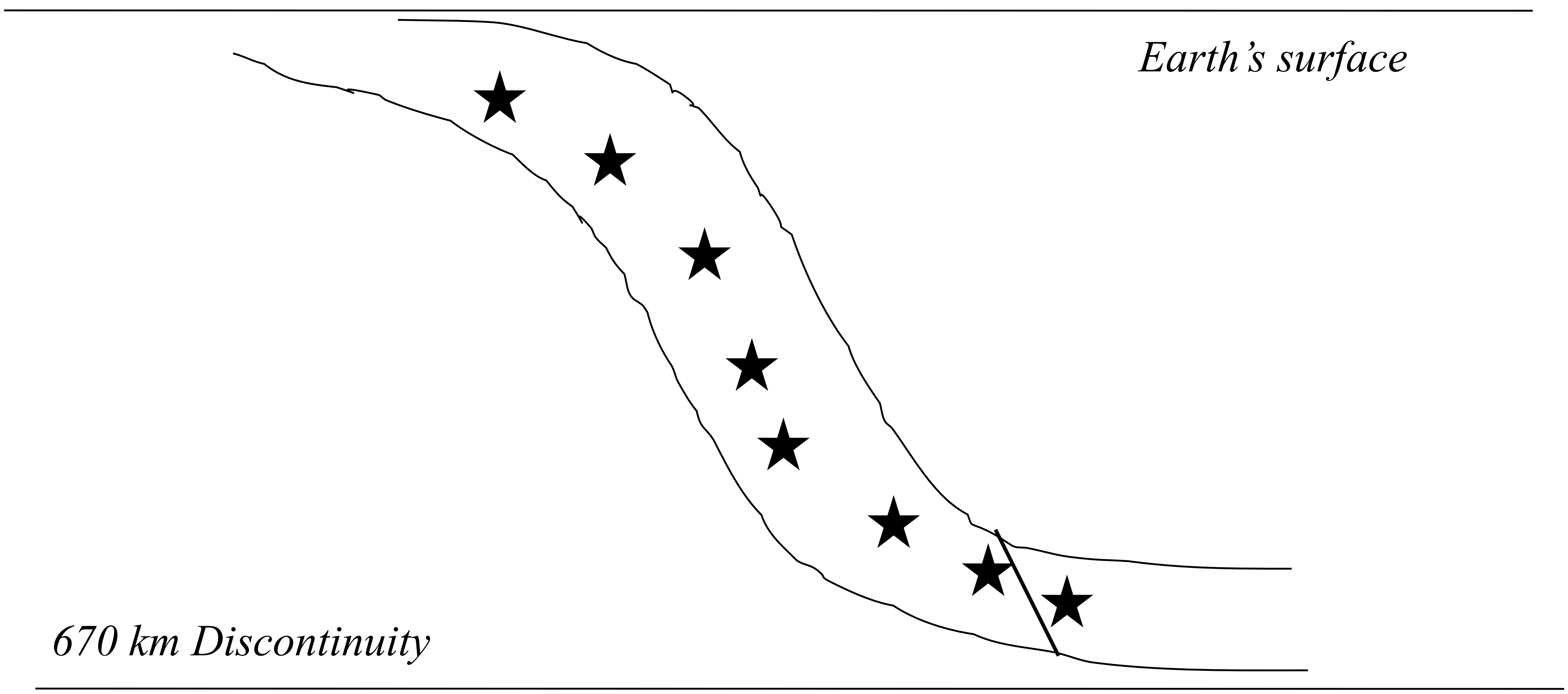

Haskell dislocation model

Haskell N. A. (1964). Total energy spectral density of elastic wave radiation from propagating faults, Bull. Seism. Soc. Am. **54**, 1811-1841

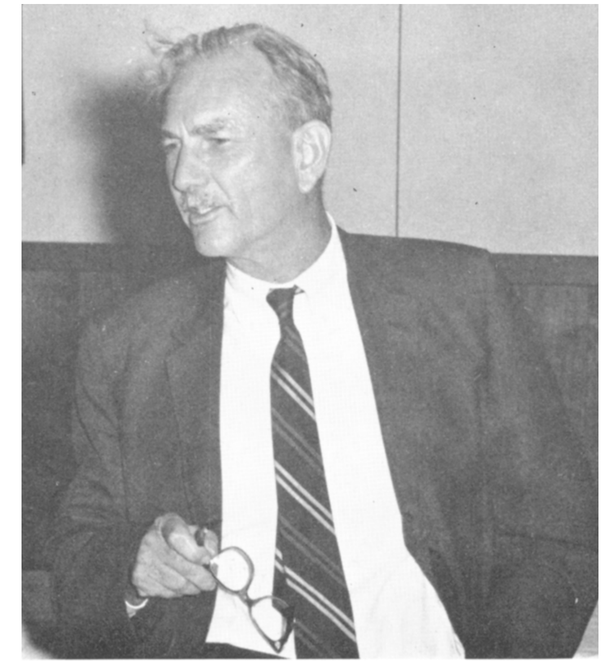

Norman A. Haskell

Rupture

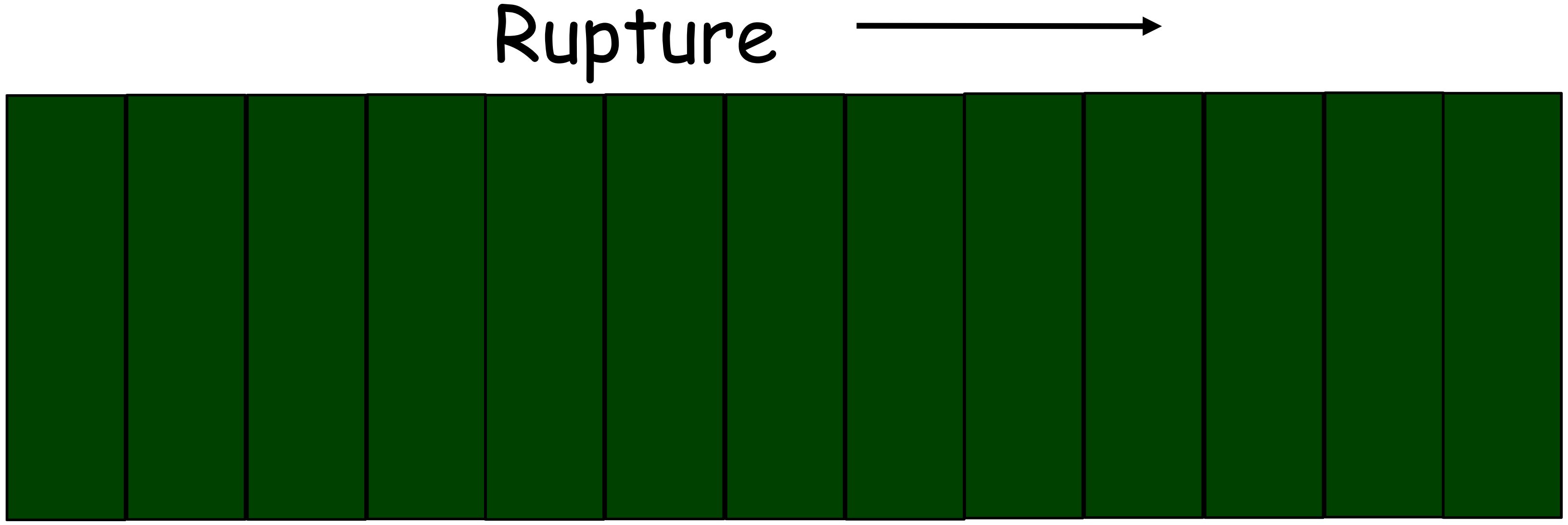

Sumatra earthquake, Dec 28, 2004

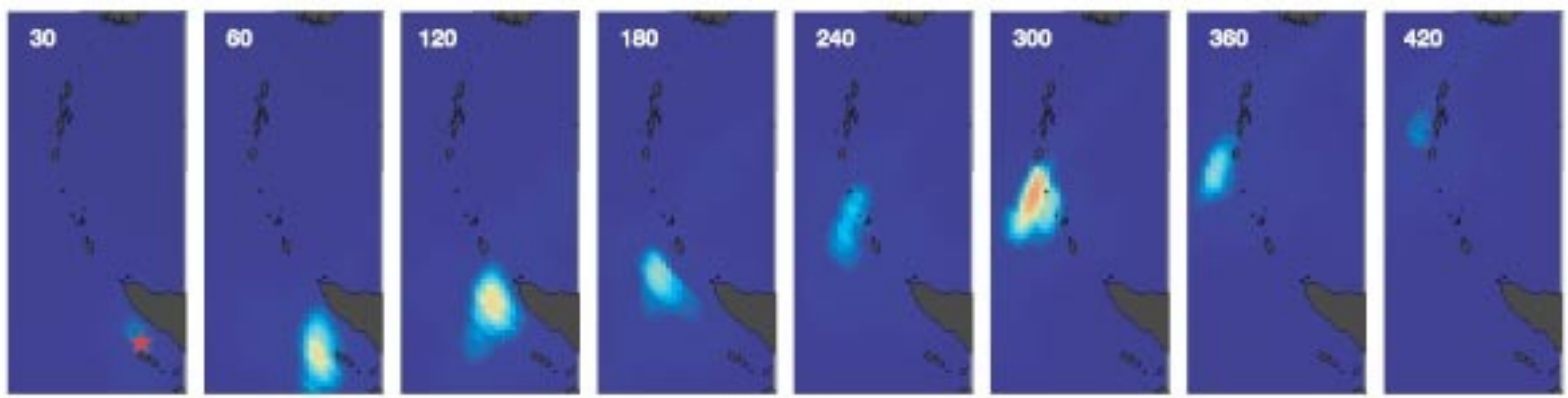

Ishii et al., Nature 2005 doi:10.1038/nature03675

Haskell source model: far field

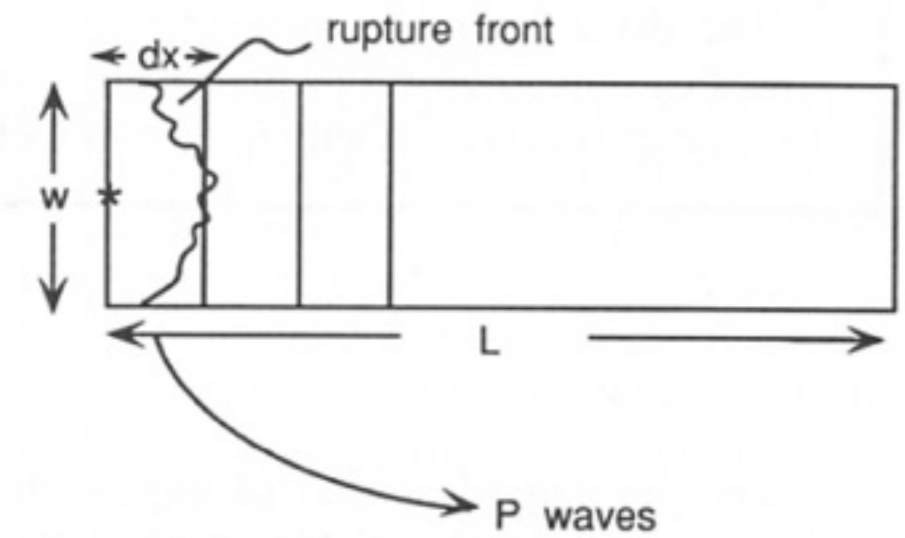

FIGURE 9.5 Geometry of a one-dimensional fault of width w and length L. The individual segments of the fault are of length dx, and the moment of a segment is $m\,dx$. The fault ruptures with velocity v_r.

$$u_r(r,t) = \sum_{i=1}^{N} u_i\left(r_i, t - r_i/\alpha - \Delta t_i\right) =$$

$$= \frac{R_i^P \mu}{4\pi\rho\alpha^3} W \sum_{i=1}^{N} \frac{\dot{D}_i}{r_i}\left(t - \Delta t_i\right) dx \approx$$

$$\approx \frac{R_i^P \mu}{4\pi\rho\alpha^3} \frac{W}{r} \sum_{i=1}^{N} \dot{D}(t) * \delta\left(t - \frac{x}{v_r}\right) dx \approx$$

$$\approx \frac{R_i^P \mu}{4\pi\rho\alpha^3} \frac{W}{r} \dot{D}(t) * \int_0^x \delta\left(t - \frac{x}{v_r}\right) dx =$$

$$= \frac{R_i^P \mu}{4\pi\rho\alpha^3} \frac{W}{r} v_r \dot{D}(t) * B(t;T_r)$$

Haskell source model: far field

$$u_r(r,t) \propto \dot{D}(t) * v_r H(z)\Big|_{t-x/v_r}^{t} = v_r \dot{D}(t) * B(t;T_r)$$

resulting in the convolution of two boxcars: the first with duration equal to the rise time and the second with duration equal to the **rupture time** (L/v_r)

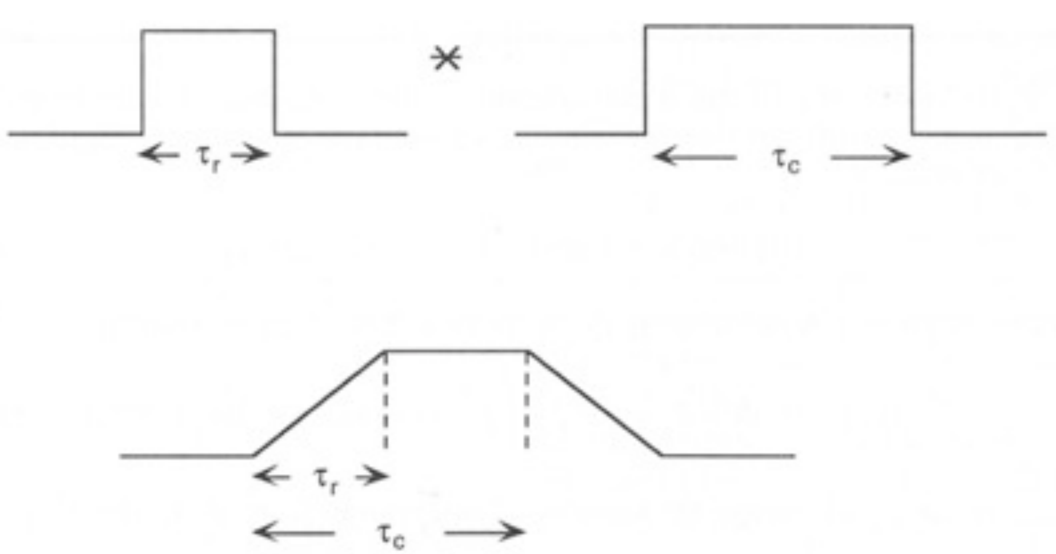

FIGURE 9.6 The convolution of two boxcars, one of length τ_r and the other of length τ_c ($\tau_c > \tau_r$). The result is a trapezoid with a rise time of τ_r, a top of length $\tau_c - \tau_r$, and a fall of width τ_r.

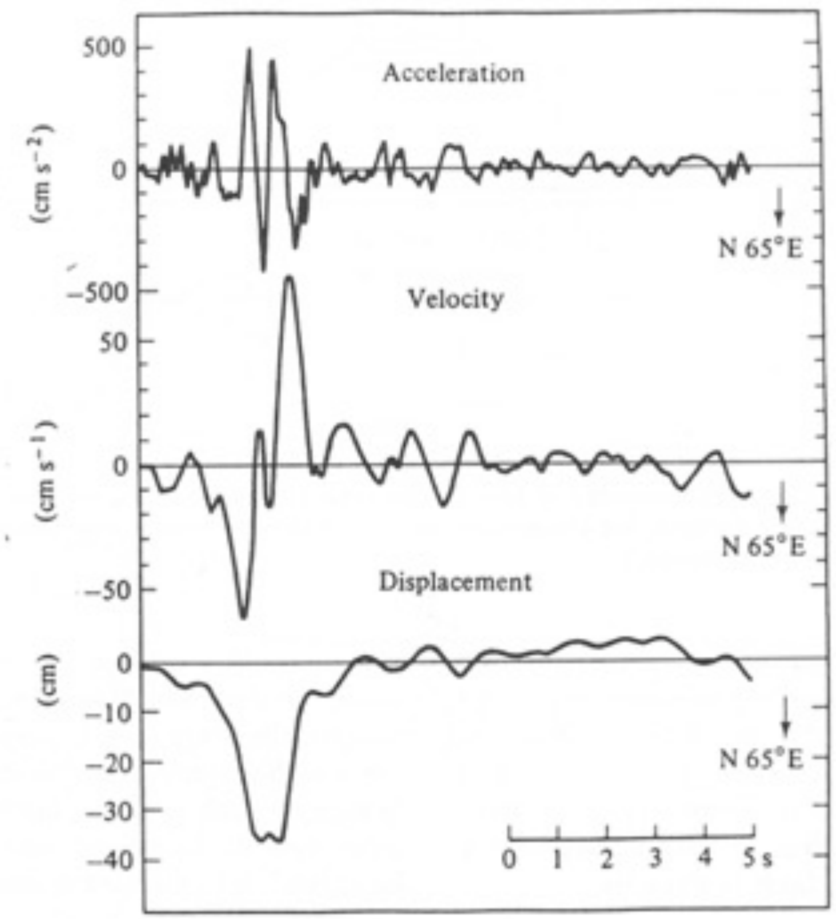

FIGURE 9.7 A recording of the ground motion near the epicenter of an earthquake at Parkfield, California. The station is located on a node for *P* waves and a maximum for *SH*. The displacement pulse is the *SH* wave. Note the trapezoidal shape. (From Aki, *J. Geophys. Res.* 73, 5359–5375, 1968; © copyright by the American Geophysical Union.)

Haskell source model: directivity

The body waves generated from a breaking segment will arrive at a receiver before than those that are radiated by a segment that ruptures later.

If the path to the station is not perpendicular, the waves generated by different segments will have different path lengths, and then unequal travel times.

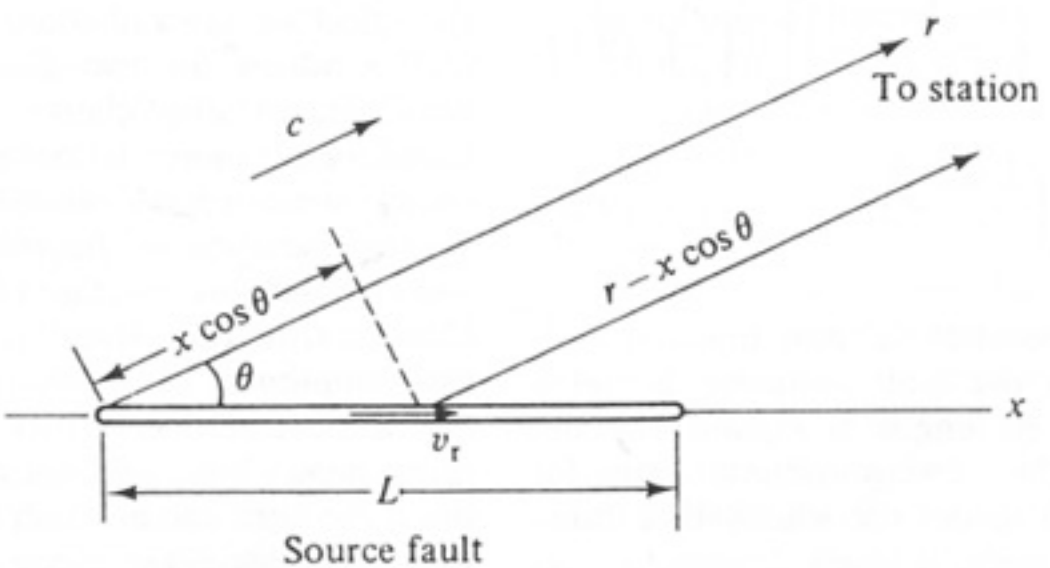

FIGURE 9.8 Geometry of a rupturing fault and the path to a remote recording station. (From Kasahara, 1981.)

$$T_r = \left[\frac{L}{v_r} + \left(\frac{r - L\cos\theta}{c}\right)\right] - \frac{r}{c} =$$

$$= \frac{L}{v_r} - \left(\frac{L\cos\theta}{c}\right) = \frac{L}{v_r}\left(1 - \frac{v_r}{c}\cos\theta\right)$$

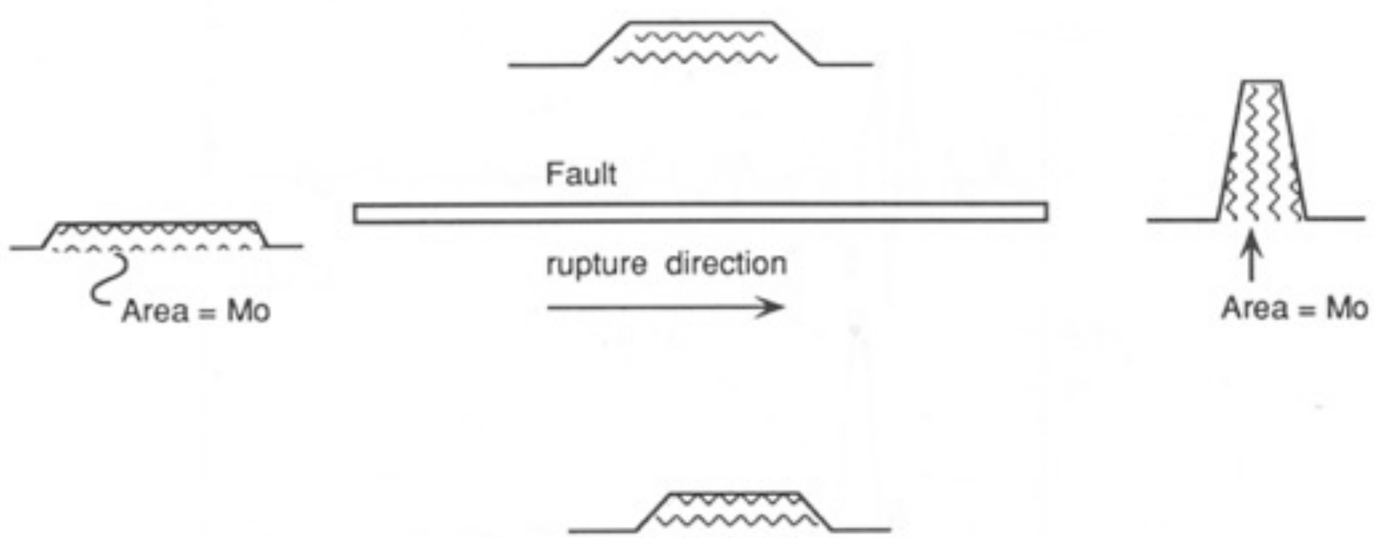

FIGURE 9.9 Azimuthal variability of the source time function for a unilaterally rupturing fault. The duration changes, but the area of the source time function is the seismic moment and is independent of azimuth.

Rupture velocity

Earthquake ruptures typically propagate at velocities that are in the range 70–90% of the S-wave velocity and this is independent of earthquake size. A small subset of earthquake ruptures appear to have propagated at speeds greater than the S-wave velocity. These supershear earthquakes have all been observed during large strike-slip events.

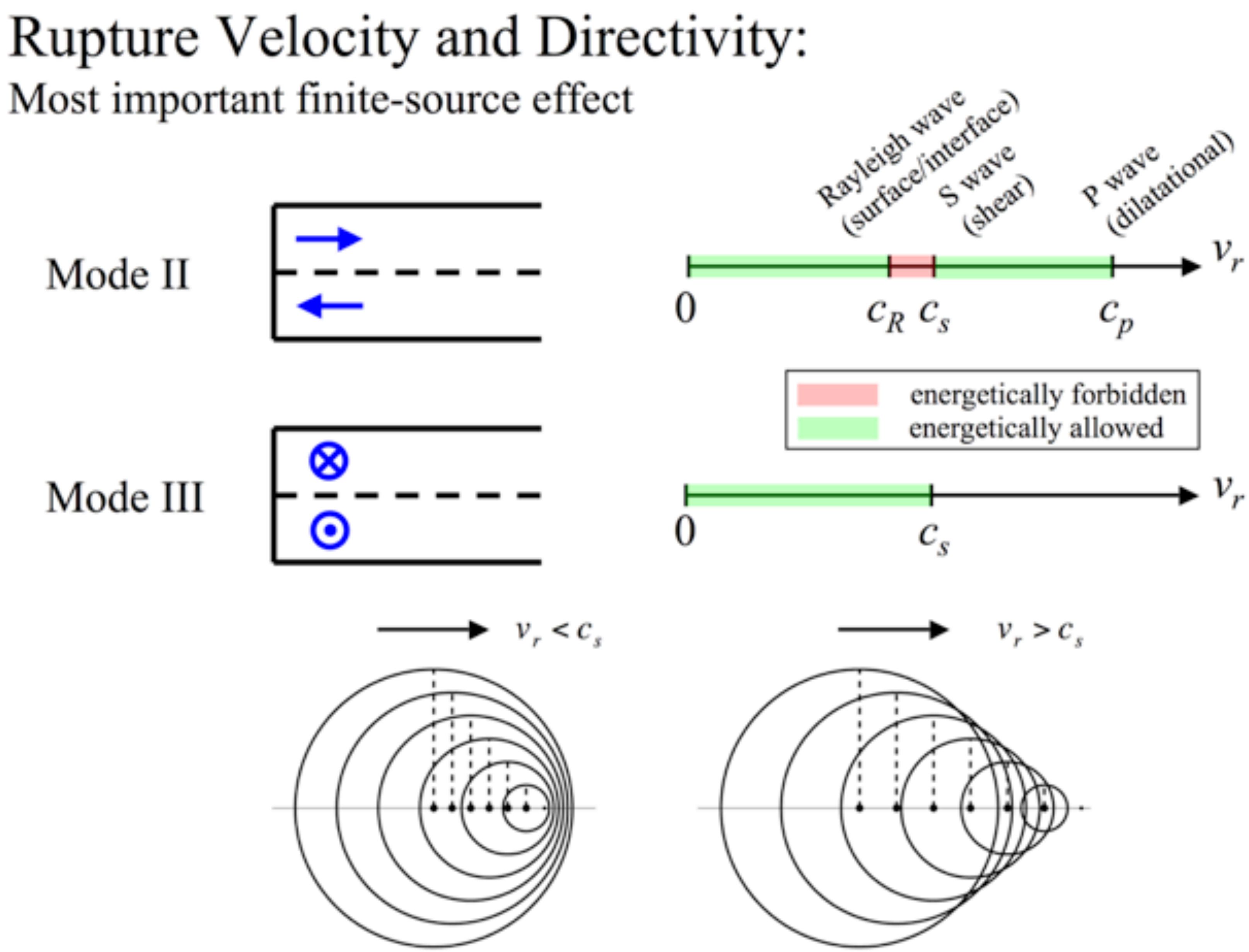

http://pangea.stanford.edu/~edunham/research/supershear.html

Directivity example

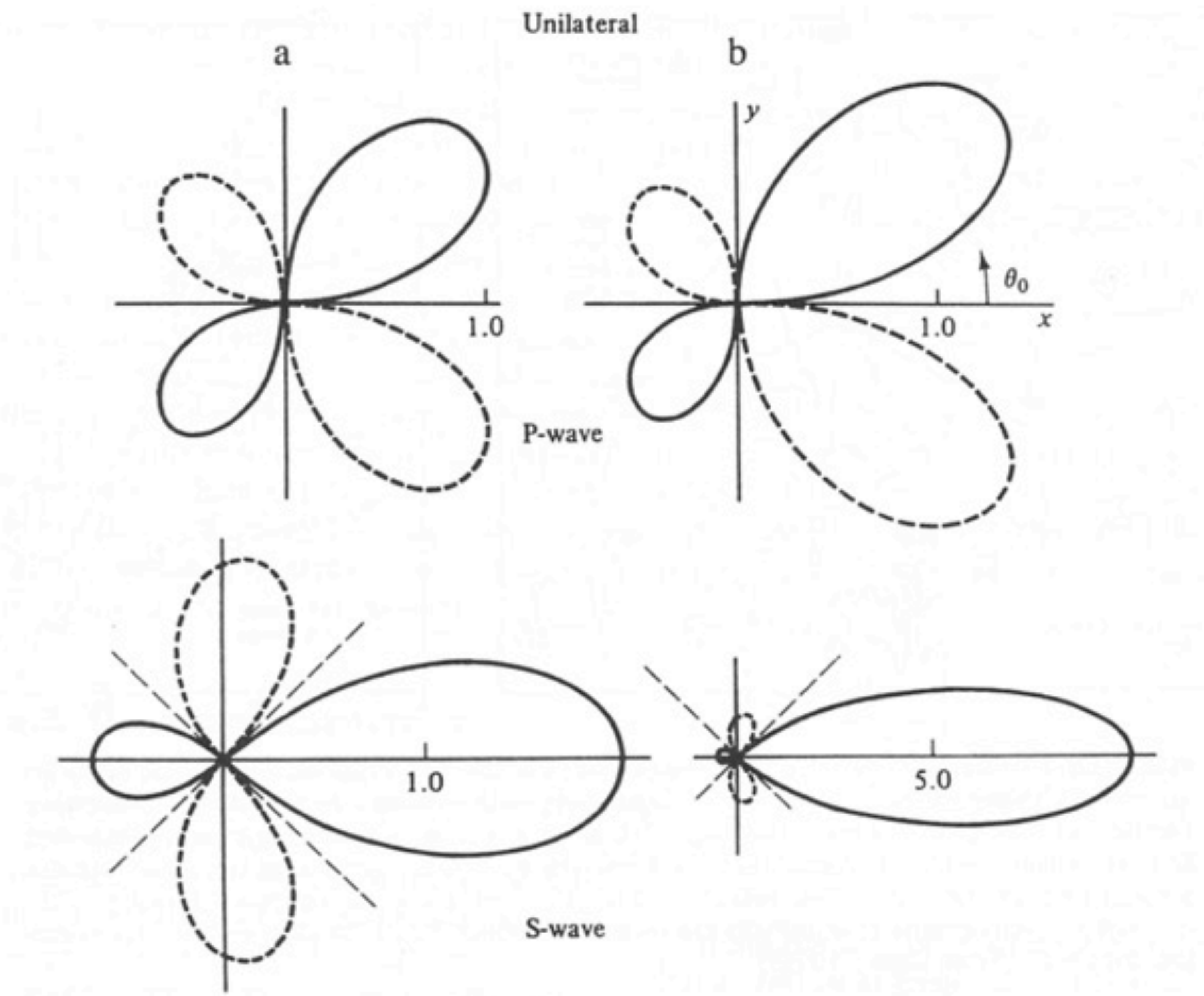

FIGURE 9.10 The variability of *P*- and *SH*-wave amplitude for a propagating fault (from left to right). For the column on the left $v_r/v_s = 0.5$, while for the column on the right $v_r/v_s = 0.9$. Note that the effects are amplified as rupture velocity approaches the propagation velocity. (From Kasahara, 1981.)

Ground motion scenarios

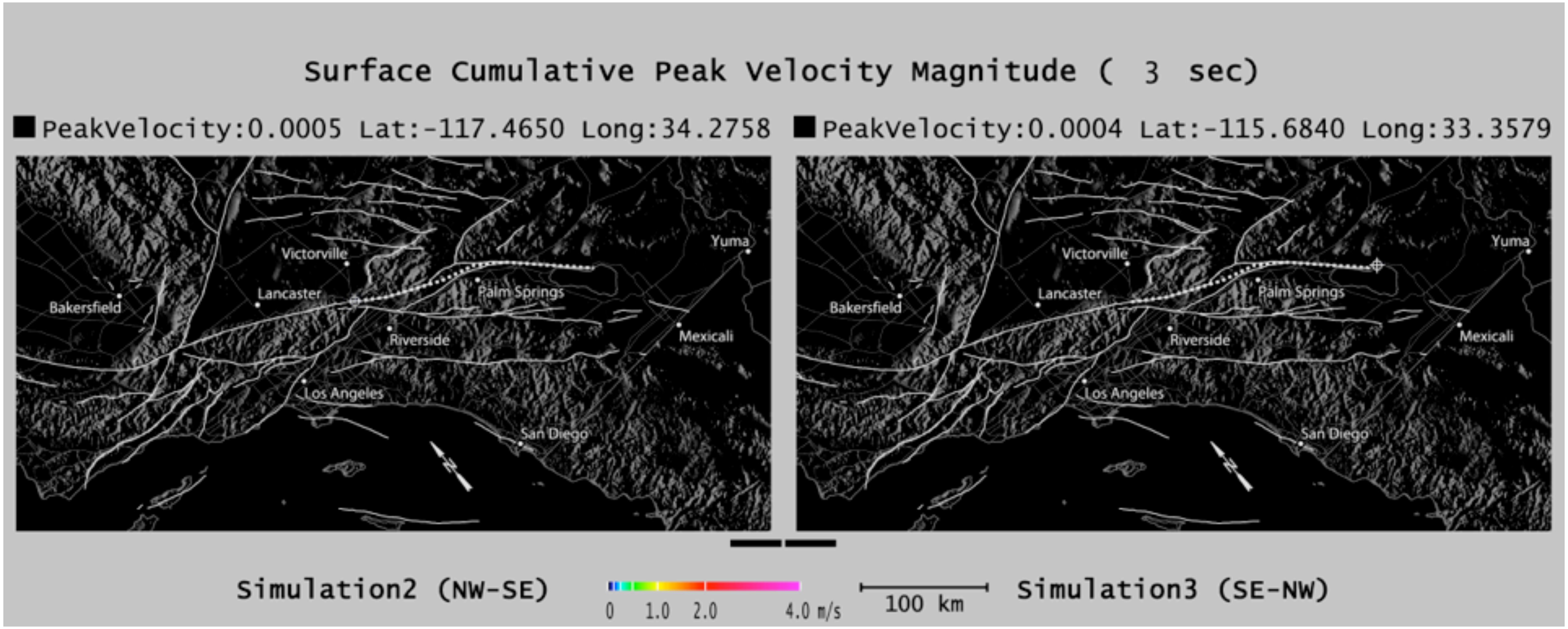

The two views in this movie show the cumulative velocities for a San Andreas earthquake TeraShake simulation, rupturing south to north and north to south. The crosshairs pinpoint the peak velocity magnitude as the simulation progresses.

www.scec.org

Source spectrum

The displacement pulse, corrected for the geometrical spreading and the radiation pattern can be written as:

$$u(t) = M_0\left(B(t;\tau) * B(t;T_R)\right)$$

and in the frequency domain:

$$U(\omega) = M_0 F(\omega) = M_0 \left|\frac{\sin\left(\frac{\omega\tau}{2}\right)}{\left(\frac{\omega\tau}{2}\right)}\right| \left|\frac{\sin\left(\frac{\omega L}{v_r 2}\right)}{\left(\frac{\omega L}{v_r 2}\right)}\right| \approx \begin{cases} M_0 & \omega < \frac{2}{T_r} \\ \frac{2M_0}{\omega T_R} & \frac{2}{T_r} < \omega < \frac{2}{\tau} \\ \frac{4M_0}{\omega^2 \tau T_R} & \omega > \frac{2}{\tau} \end{cases}$$

Source spectrum

$$U(\omega) \approx \begin{cases} \boxed{M_0} & \omega < \dfrac{2}{T_r} \\ \boxed{\dfrac{2M_0}{\omega T_R}} & \dfrac{2}{T_r} < \omega < \dfrac{2}{\tau} \\ \boxed{\dfrac{4M_0}{\omega^2 \tau T_R}} & \omega > \dfrac{2}{\tau} \end{cases}$$

Figure 4.6-4: Approximation of the (sin *x*)/*x* function, and derivation of corner frequencies.